# Cold Nuclear Effects on Quarkonium Production at RHIC

**R. Vogt**

**Lawrence Livermore National Laboratory, Livermore, CA 94551, USA**

**Physics Department, University of California, Davis, CA 95616, USA**

# Cold Nuclear Matter?

**Cold matter effects are non-QGP effects: form baseline features of nuclear collisions**

**Quarkonium production is a hard process, calculable in perturbative QCD**

**Hard processes should have a linear $A$ dependence if no nuclear effects, $\sigma_{pA} = \sigma_{pp}A$**

- **Fixed-target experiments show that $A$ dependence of $J/\psi$ production is less than linear**
- **$J/\psi$ and $\psi'$ $A$ dependencies are different**
- **Inclusive $J/\psi$ has contributions from $\chi_c$ and $\psi'$ feed down**
- **Initial-state parton distributions in nuclei are different than in free protons**

# $A$ Dependence of $J/\psi$ and $\psi'$ Not Identical

Extensive fixed-target data sets (NA50 at SPS, E866 at FNAL) show clear difference at midrapidity [NA50 $\rho L$ fit gives $\Delta\sigma = \sigma_{\rm abs}^{\psi'} - \sigma_{\rm abs}^{J/\psi} = 4.2 \pm 1.0$ mb at 400 GeV, $2.8 \pm 0.5$ mb at 450 GeV for absolute cross sections]

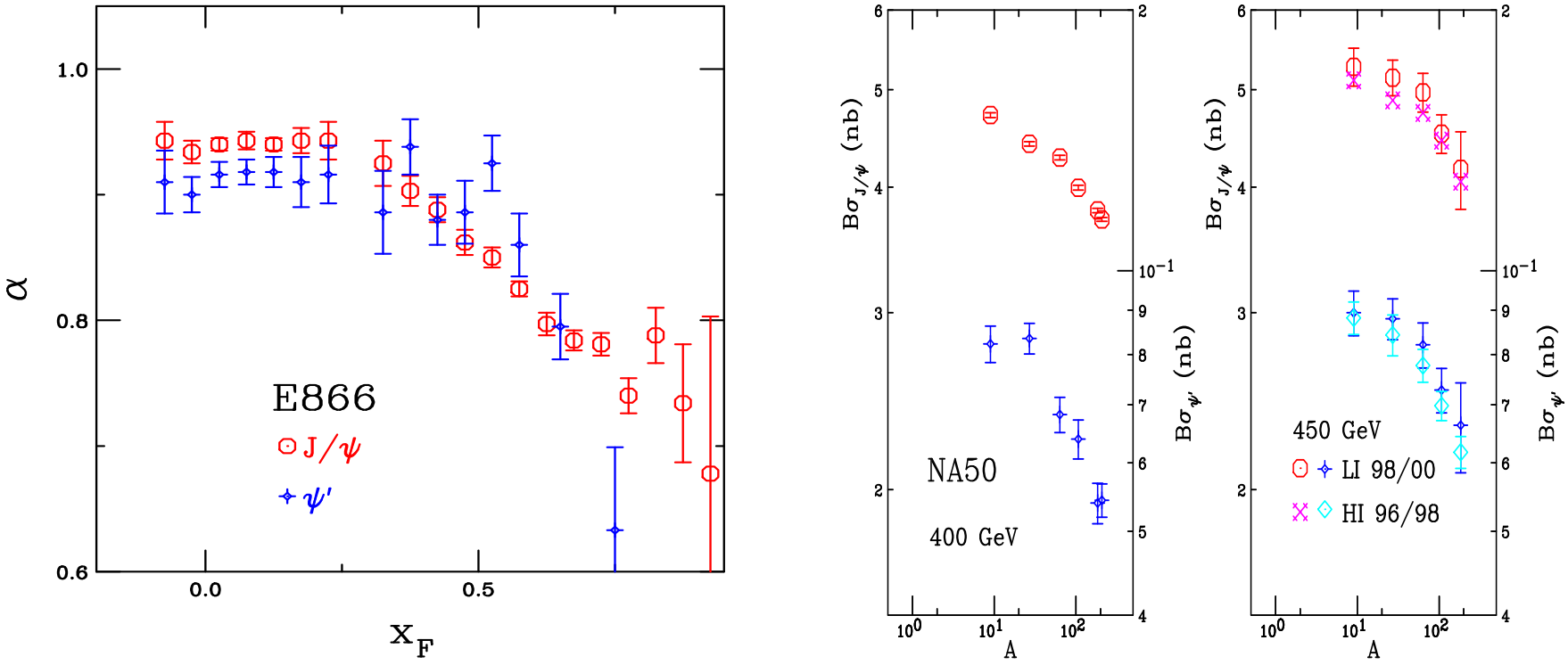


Figure 1: The $J/\psi$ $A$ dependence (left) as a function of $x_F$ at FNAL ($\sqrt{S_{NN}} = 38.8$ GeV) and (right) and a function of $A$ at the SPS (NA50 at $p_{\rm lab} = 400$ and 450 GeV) for $J/\psi$ and $\psi'$ production.

# Feed down Contributions to Inclusive $J/\psi$

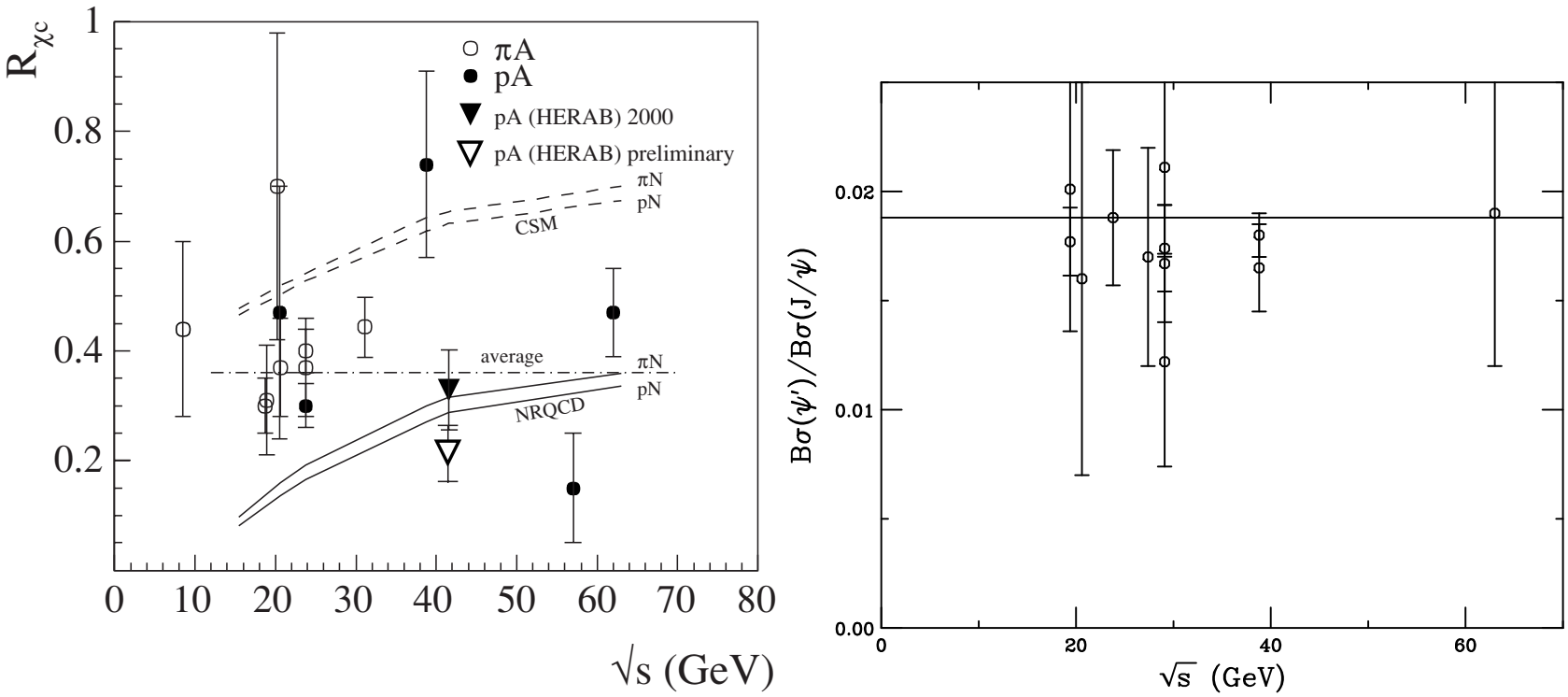


Figure 2: Left: Ratio of $\chi_c$ to $J/\psi$ cross sections as a function of $\sqrt{S}$ for $\pi A$ and $pA$ fixed-target measurements. The CSM and NRQCD curves are obtained from Monte Carlo while the 'average' is the average value of all measurements. From I. Abt *et al.* (HERA-B Collab.), Phys. Lett. **561** (2003) 61. Right: Ratio of $\psi'$ to $J/\psi$ cross sections to lepton pairs as a function of $\sqrt{S}$ for $pp$ and $pA$ measurements. Adapted from R.V., Phys. Rept. **310** (1999) 197.

# Parton Densities Modified in Nuclei

Nuclear deep-inelastic scattering measures quark modifications directly, gluon modifications only through $Q^2$ dependence of $F_2$

More uncertainty in nuclear gluon distribution

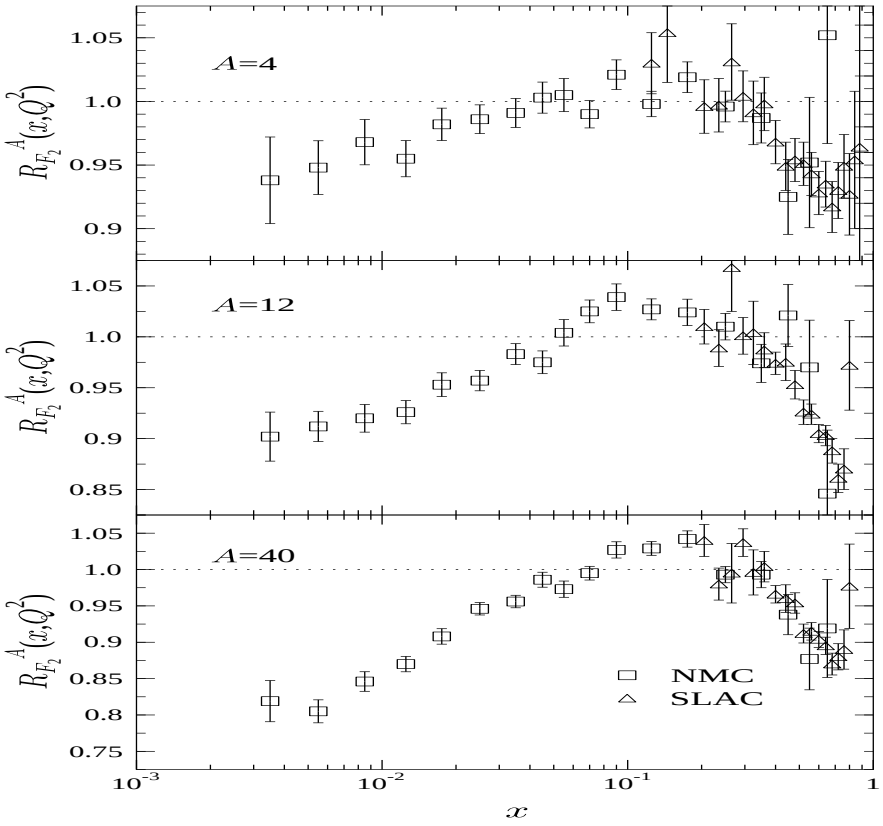


Figure 3: Ratios of charged parton densities in He, C, and Ca to D as a function of $x$. [From K.J. Eskola.]

# Nuclear Parton Distributions

**Nuclear parton densities**

$$\begin{aligned} F_i^A(x,Q^2,\vec{r},z) &= \rho_A(s) S^i(A,x,Q^2,\vec{r},z) f_i^N(x,Q^2) \\ s &= \sqrt{r^2+z^2} \\ \rho_A(s) &= \rho_0 \frac{1+\omega(s/R_A)^2}{1+\exp[(s-R_A)/d]} \end{aligned}$$

**With no nuclear modifications,** $S^i(A,x,Q^2,\vec{r},z) \equiv 1$

**Use Eskola *et al.* (EKS98 and EPS08) and DeFlorian & Sassot (nDSg) parameterizations**

Assume spatial dependence proportional to nuclear path length:

$$S_\rho^i(A,x,Q^2,\vec{r},z) = 1 + N_\rho(S^i(A,x,Q^2)-1)\frac{\int dz \rho_A(\vec{r},z)}{\int dz \rho_A(0,z)}$$

**Normalization:** $(1/A)\int d^2r dz \rho_A(s) S_\rho^i \equiv S^i$

**Larger than average modifications for** $s = 0$

**Nucleons like free protons when** $s \gg R_A$

# Comparing Shadowing Parameterizations: $x$ Dependence

**EKS98, EPS08 and nDSg available for all $A$, HKN for select nuclei**

**EKS98 and EPS08 have strong antishadowing at $x \sim 0.1$, nDSg has almost none**
**EPS08 stronger at low $x$ than others to fit forward data $A$**

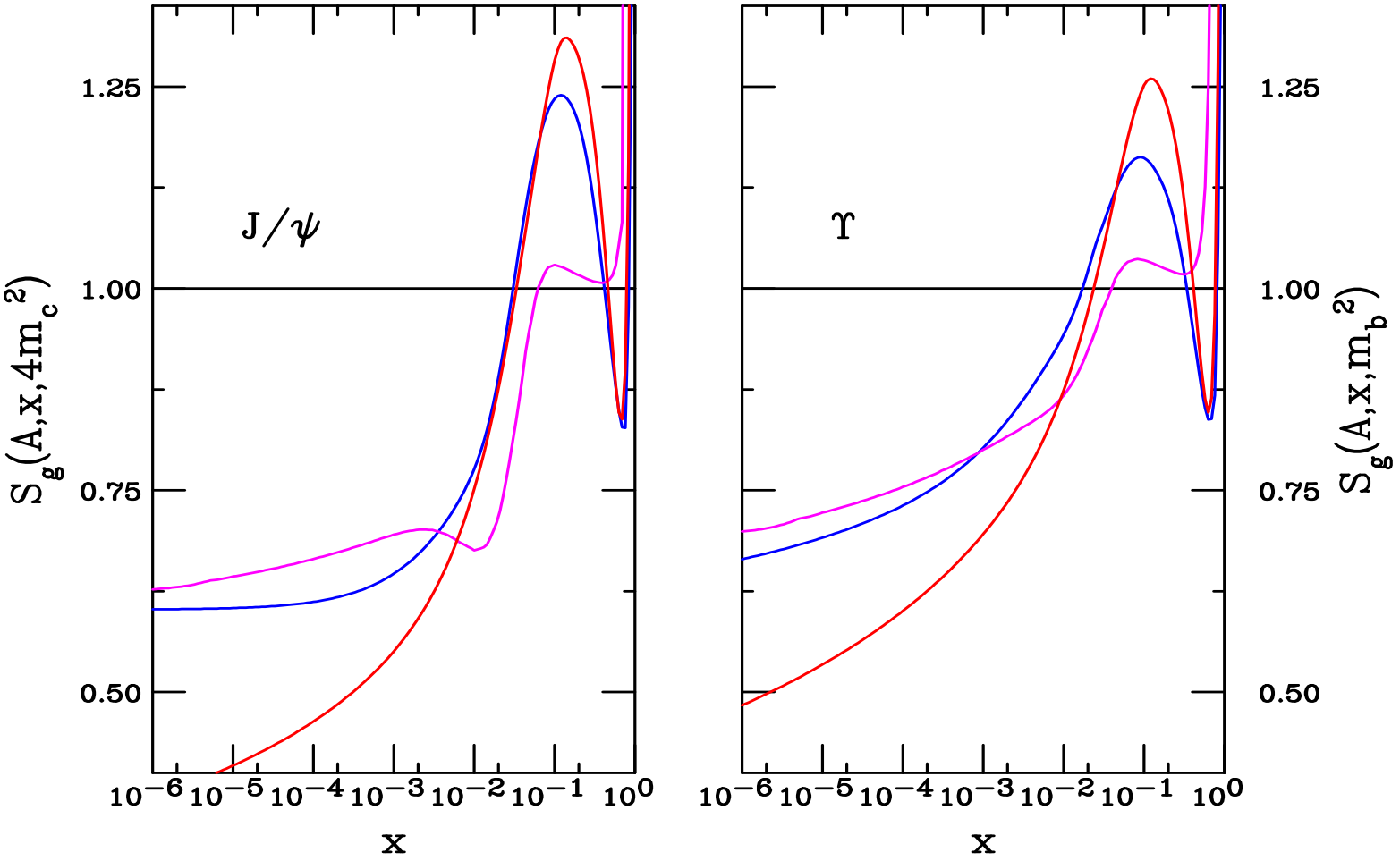


Figure 4: EKS98 (blue), nDSg (magenta), and EPS08 (red) gluon shadowing parameterizations for $J/\psi$ production scales for $A$ =Au.

# Average $x_2$ as a Function of Energy and Rapidity

$\langle x_2 \rangle$ as a function of rapidity for $2 \to 2$ scattering (N.B. $\langle x_1 \rangle$ is mirror imagine of $\langle x_2 \rangle$)

Increasing $\sqrt{S}$ broadens $y$ range and decreases $x_2$

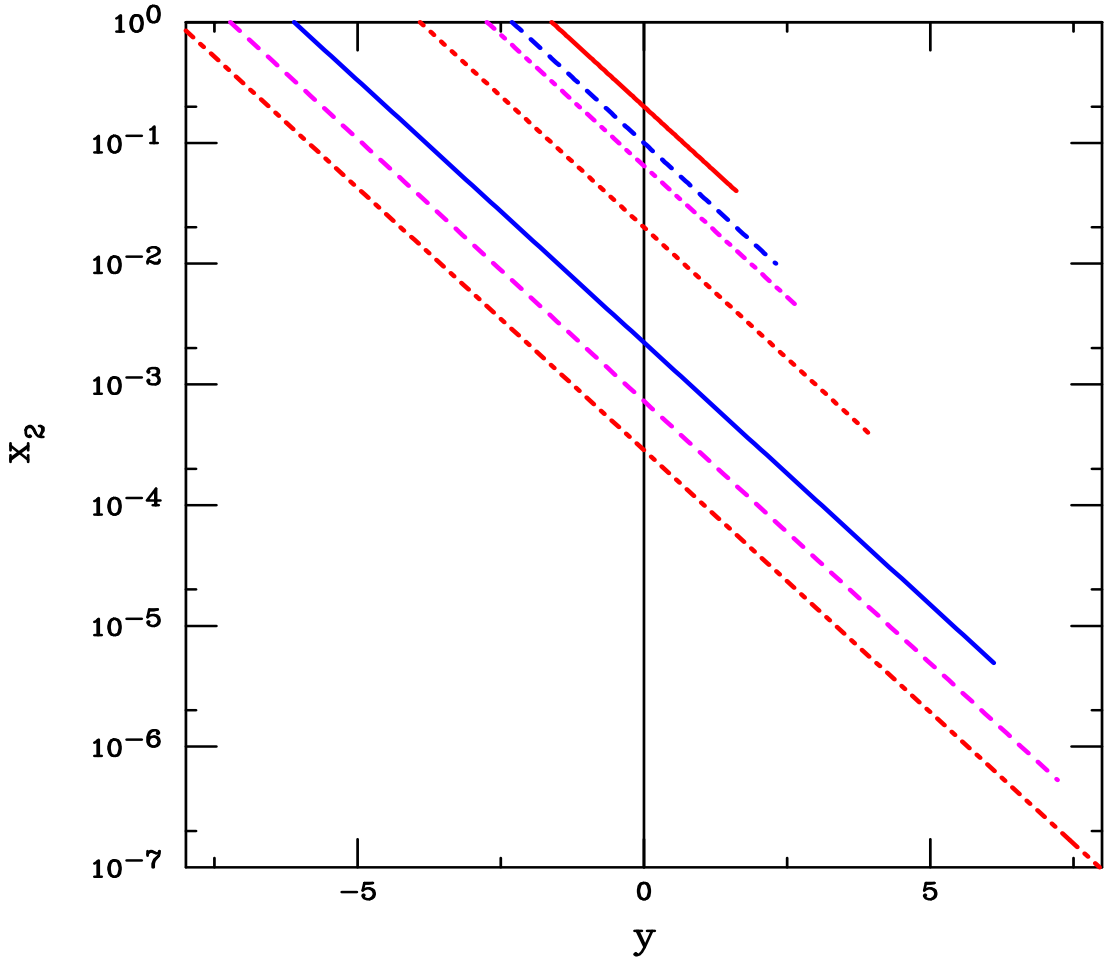


Figure 5: We give the average value of the nucleon momentum fraction, $x_2$, in $pp$ collisions as a function of rapidity for (top to bottom) $\sqrt{S_{NN}} = 20$; 40; 62; 200; 1800; 5500 and 14000 GeV.

# Quarkonium Absorption by Nucleons

**Woods-Saxon nuclear density profiles typically used**

$$\begin{aligned}\sigma_{pA} &= \sigma_{pN}\int d^2b \int_{-\infty}^{\infty} dz\, \rho_A(b,z) S_A^{\rm abs}(b) \\ &= \sigma_{pN}\int d^2b \int_{-\infty}^{\infty} dz\, \rho_A(b,z) \exp\left\{-\int_z^{\infty} dz' \rho_A(b,z')\sigma_{\rm abs}(z'-z)\right\}\end{aligned}$$

**Note that if** $\rho_A = \rho_0$, $\alpha = 1 - 9\sigma_{\rm abs}/(16\pi r_0^2)$

**The value of** $\sigma_{\rm abs}$ **depends on the parameterization of** $\sigma_{pA}$ **– Glauber, hard sphere,** $A^\alpha$ **etc. (shown by NA50)**

**Initial-state shadowing not taken into account at SPS energies,**
**increasing** $\sqrt{S_{NN}}$ **and rapidity range of measurement influences total shadowing effect: could make effective** $\sigma_{\rm abs}$ **without shadowing depend on** $y$, $\sqrt{S_{NN}}$

**Feed down to** $J/\psi$ **from** $\chi_c$ **and** $\psi'$ **decays included: assume 60% direct** $J/\psi$, **30%** $\chi_c$ **and 10%** $\psi'$ ($F_{J/\psi}^{\rm dir} = 0.6$, $F_{\chi_c} = 0.3$ **and** $F_{\psi'} = 0.1$) **[N.B. More recent HERA-B data suggest smaller** $\chi_c$ **contribution]**

$$\sigma_{pA} = \sigma_{pN}\int d^2b\, [F_{J/\psi}^{\rm dir} S_{\psi,\,\rm dir}(b) + F_{\chi_c} S_{\chi_{cJ}}(b) + F_{\psi'} S_{\psi'}(b)]$$

# Comparing Absorption Calculations

**$A^\alpha$ with $\alpha = 1 - 9\sigma_{\rm abs}/(16\pi r_0^2)$, $\sigma_{\rm abs} = 4.8$ mb is line on semi-log plot**

**Exponential survival probability with $S \propto \exp(-\rho_0 \sigma_{\rm abs} L)$ has convex shape. Using $\rho_0 = 0.16$ fm$^{-3}$ and $L = (3/4) r_0 A^{1/3}$ gives smooth curve.**

**Real nuclear shapes (points) show fluctuations due to different densities, sizes**

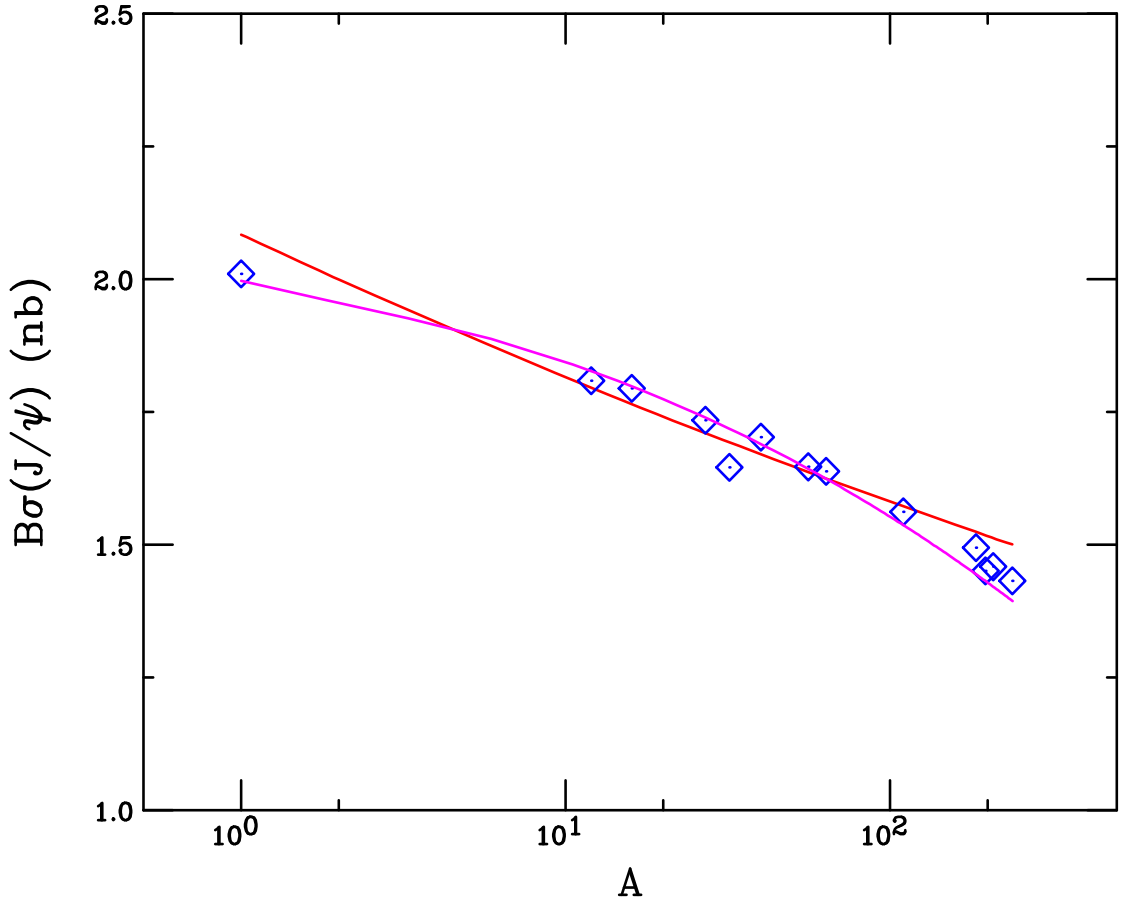


Figure 6: The $J/\psi$ $A$ dependence, all with $\sigma_{\rm abs} = 4.8$ mb, normalized to typical SPS $J/\psi$ cross section. The red line is the result for $A^\alpha$, the dashed with $\exp(-\rho_0 \sigma_{\rm abs} L)$ and the points are numerical calculations of the survival probability with real nuclear shapes.

# Nuclear Absorption Calculations

**Assume that each charmonium state interacts with a different constant asymptotic absorption cross section,**

$$\sigma_{\rm abs}^{C} = \sigma_{\rm abs}^{J/\psi}\left(\frac{r_C}{r_{J/\psi}}\right)^2$$

**While the $\chi_c$ $A$ dependence has still not been measured, the $\psi'$ $A$ dependence is stronger than the $J/\psi$**

**We take $r_{\chi c} = 1.44\, r_{J/\psi}$ $[\sigma_{\chi c} = 2.07\sigma_{J/\psi}]$ and $r_{\psi'} = 1.8\, r_{J/\psi}$ $[\sigma_{\psi'} = 3.24\sigma_{J/\psi}]$ (Satz)**

**Measurements from SPS to RHIC suggest that absorption decreases with increasing energy while shadowing effects increase**

**Predictions that quarkonium absorption cross sections decrease with energy agree with trend of data [M. A. Braun *et al.*, Nucl. Phys. B 509 (1998) 357 (hep-ph/9707424), A. Capella and E. G. Ferreiro (hep-ph/0610313)]**

**Absorption alone always gives less than linear $A$ dependence ($\alpha < 1$)**

# Interplay of Shadowing and Absorption

**Depending on $x$ values probed, including shadowing can enhance or reduce absorption cross section needed to describe data**

**For SPS energies, $17.3 \leq \sqrt{S} \leq 29$ GeV, rapidity range covered is in EMC and anti-shadowing region, $pA/pp > 1$ with no absorption**

**Adding shadowing to absorption calculations in this energy range means a larger absorption cross section is required for agreement with data**

**For $\sqrt{S} \geq 38$ GeV, shadowing regime, thus $pA/pp < 1$ with shadowing alone at $y > 0$, smaller absorption cross section needed to agree with data**

**Since absorption is essentially independent of rapidity with CEM in the RHIC range, initial-state shadowing and absorption survival probability factorize**

# Shadowing and Absorption at the SPS: $A$ Dependence

## Stronger antishadowing of EKS98 in SPS midrapidity region calls for bigger absorption cross section

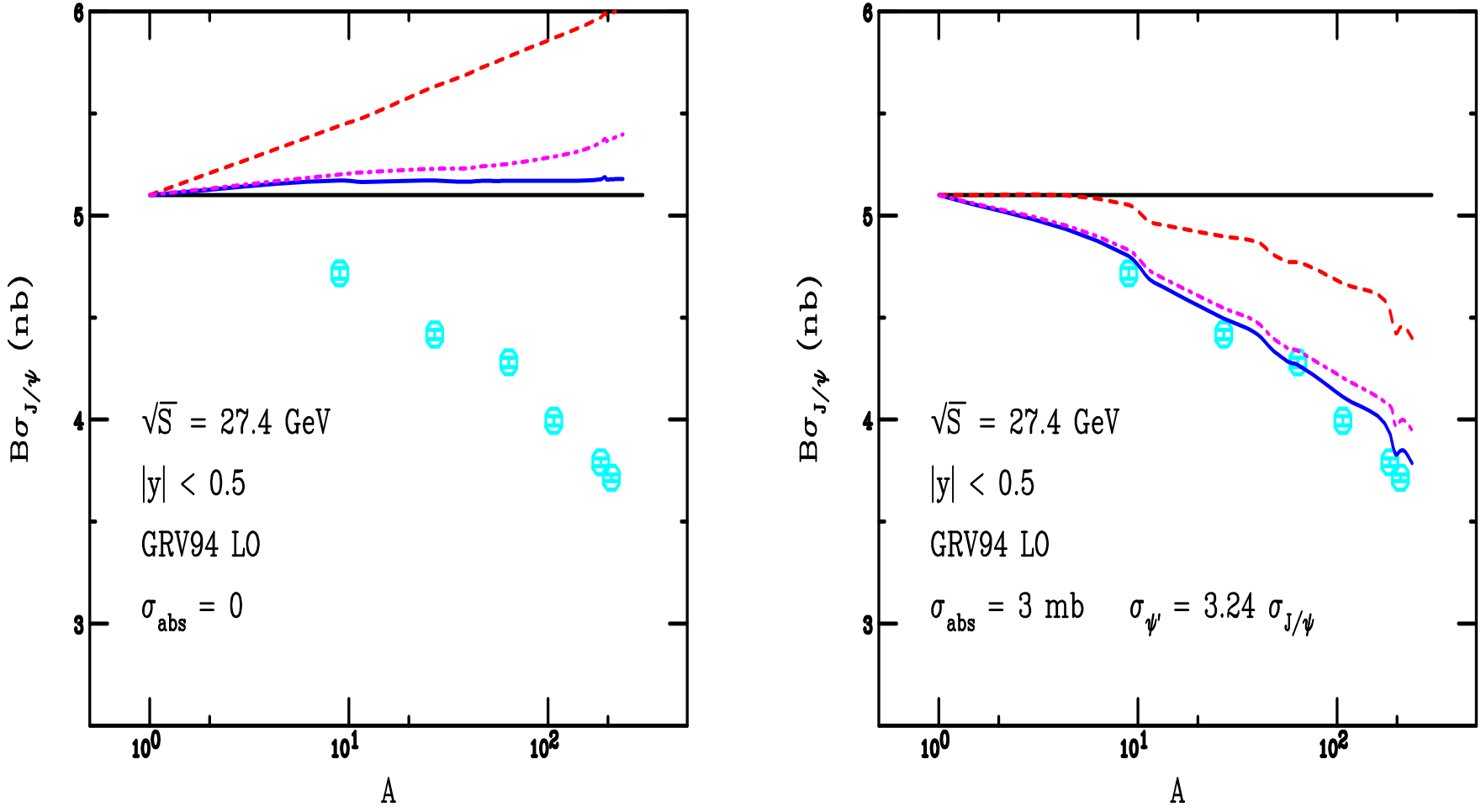


Figure 7: The $J/\psi$ $A$ dependence at 400 GeV for no absorption (left) and for $\sigma_{\rm abs}^{J/\psi} = 3$ mb (right). The curves are with no shadowing (solid blue), EKS98 (magenta dot-dashed) and nDSg(red dashed).

# Shadowing and Absorption at the SPS: $y$ Dependence

**Rapidity dependence becomes more pronounced with increasing $A$**
**Order of $R_{pA}$ per nucleon reversed when absorption added**

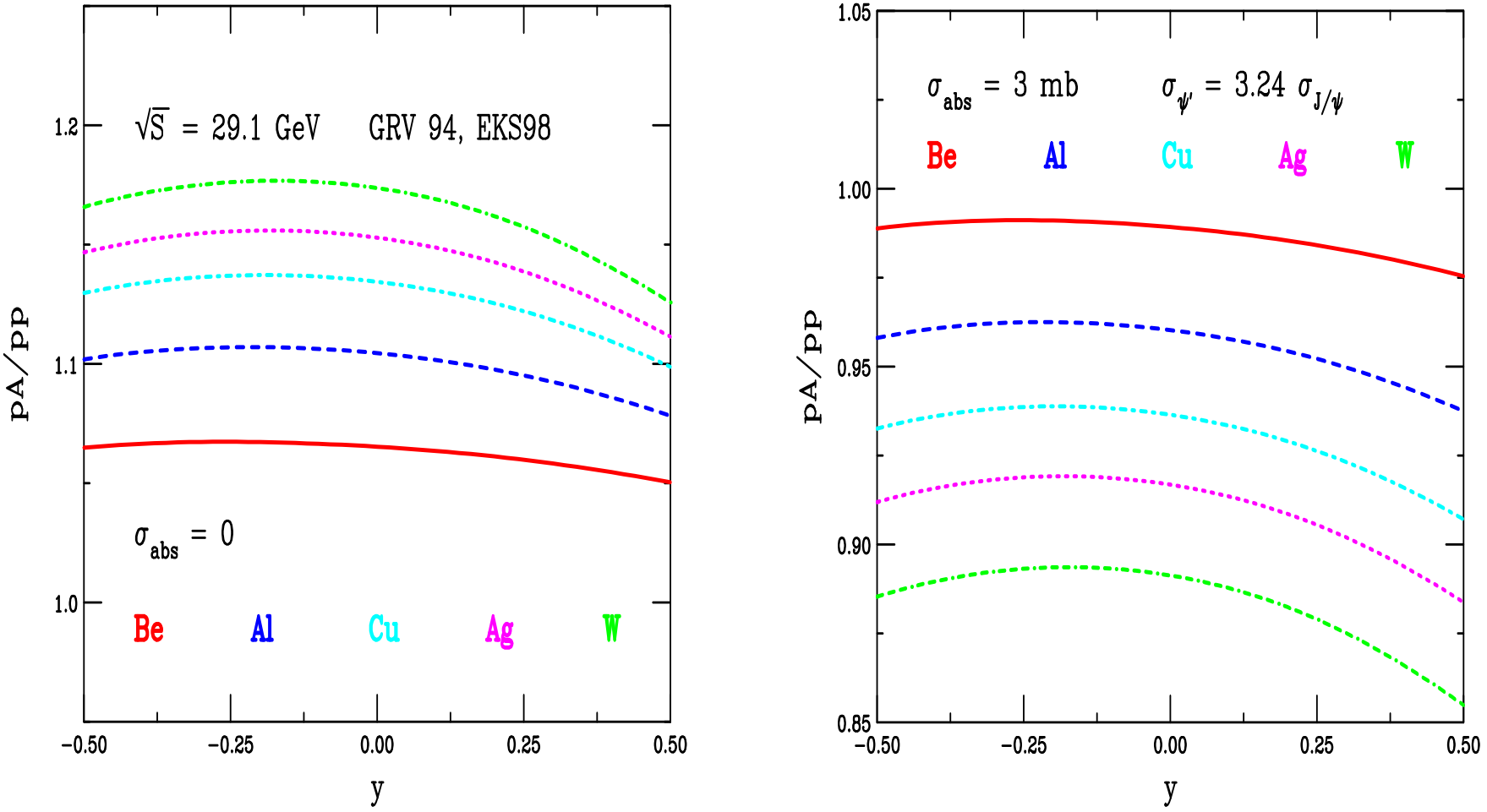


Figure 8: The $J/\psi$ $A$ dependence at 400 GeV for no absorption (left) and for $\sigma_{\rm abs}^{J/\psi} = 3$ mb (right) with the GRV 94 parton densities and EKS98 shadowing parameterization.

# Shadowing and Absorption at the SPS: $p_{\rm lab}$

## Antishadowing peak moves to left with increasing energy

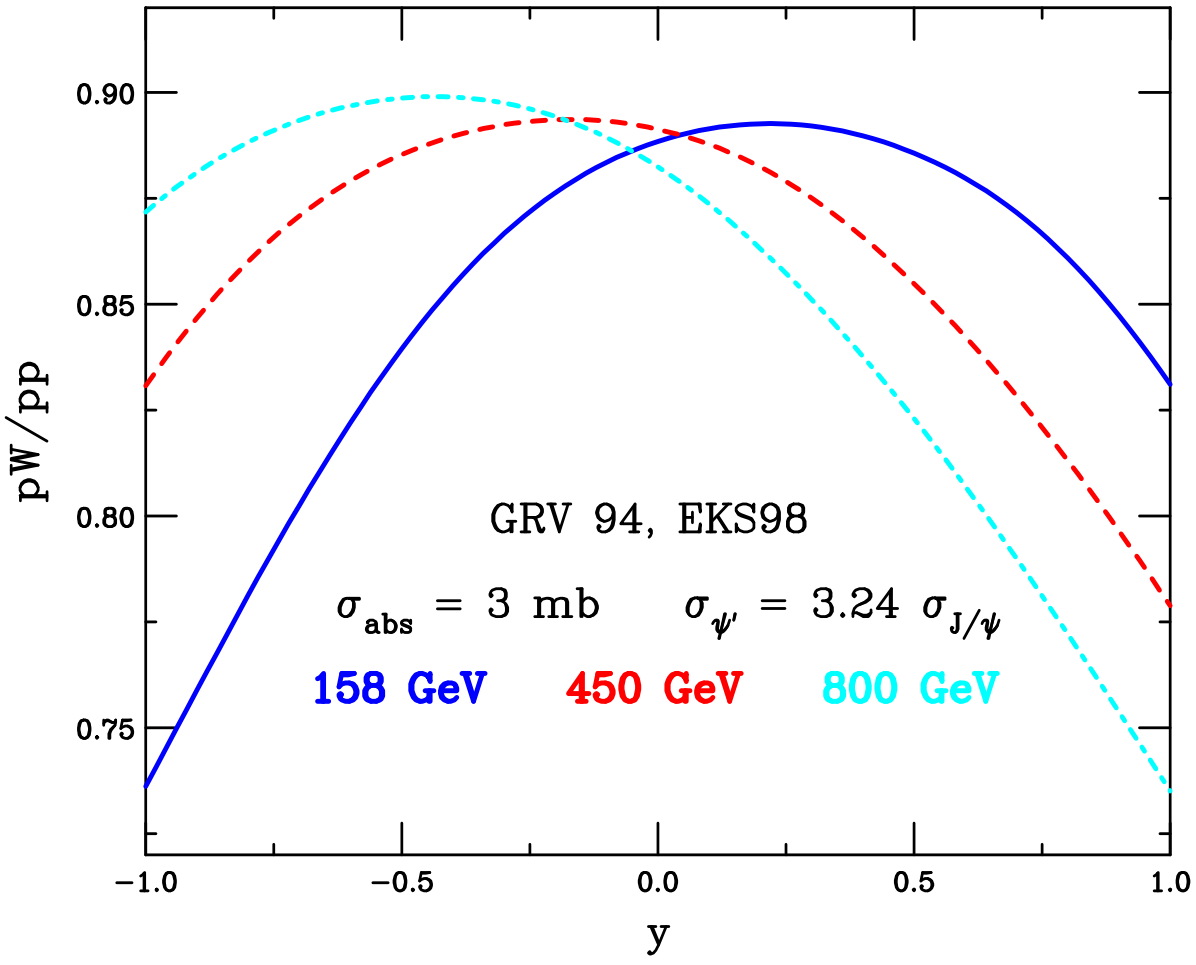


Figure 9: The $J/\psi$ $y$ dependence at 158, 450 and 800 GeV for EKS98.

# Absorption and Shadowing at RHIC: $R_{\rm dAu}(y)$

**Feed down from higher states with larger absorption cross sections requires $\sigma_{\rm abs}^{J/\psi} < 2$ mb with d+Au data**

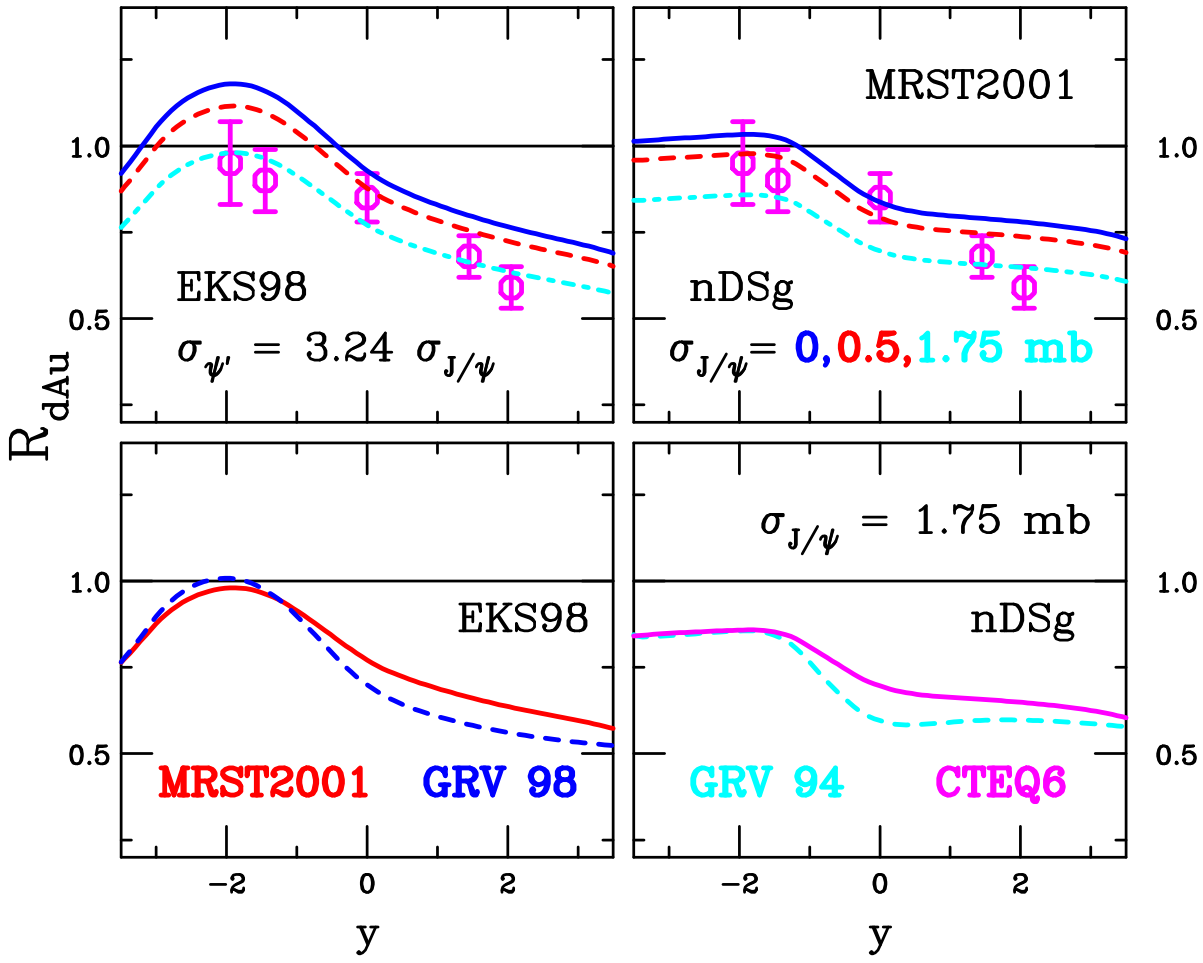


Figure 10: The d+Au/$pp$ minimum bias ratio as a function of rapidity for the EKS98 (left) and nDSg (right) parameterizations. The top plots vary the $J/\psi$ absorption cross section with the MRST2001 PDFs while the bottom plots show the differences in the PDF choice for a fixed absorption cross section.

# PHENIX Fits $\sigma_{\rm breakup}$ to $R_{\rm dAu}(y)$

**PHENIX fits a constant "breakup" cross section common to all charmonium states assuming either EKS98 or nDSg shadowing**

**Required breakup cross sections are $\sigma_{\rm breakup} = 2.8\pm^{1.7}_{1.8}$ mb for EKS98 and $\sigma_{\rm breakup} = 2.2\pm^{1.6}_{1.5}$ mb for nDSg**

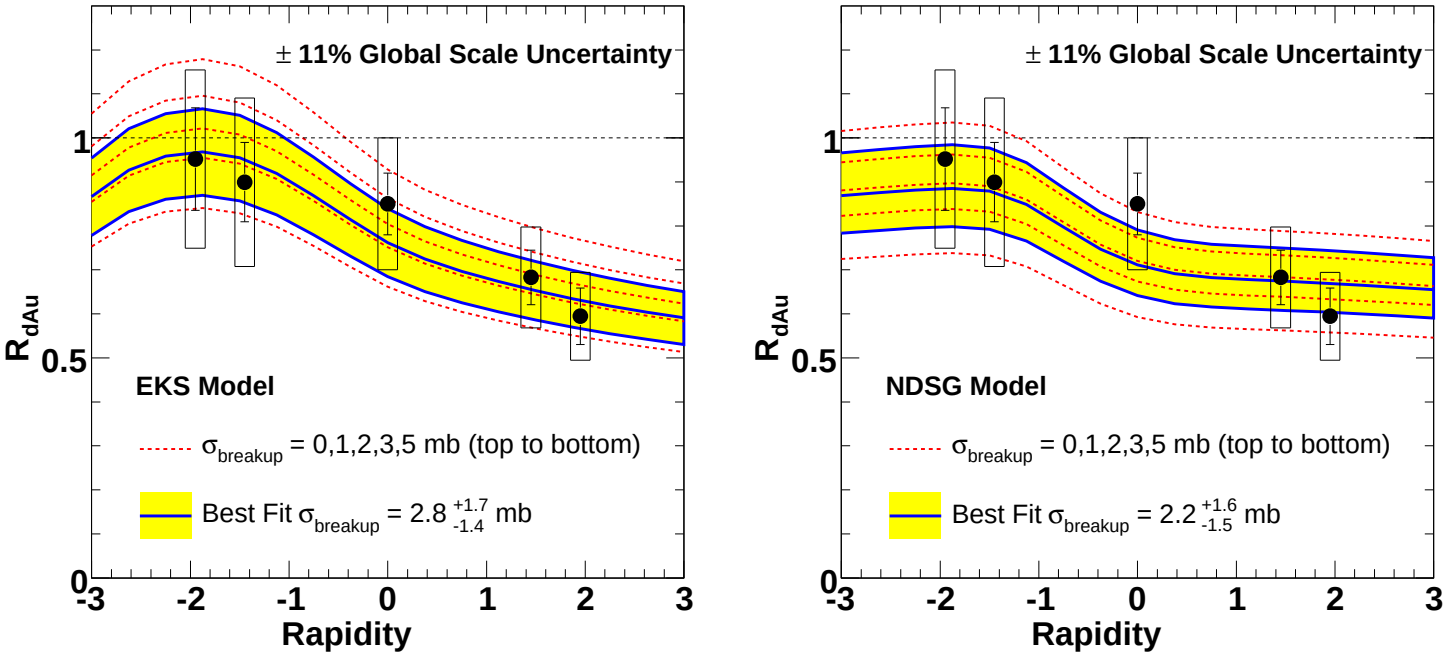


Figure 11: The d+Au/$pp$ minimum bias ratio as a function of rapidity for the EKS98 (left) and nDSg (right) parameterizations. A range of breakup cross sections ($\sigma_{\rm breakup}$ = 0, 1, 2, 3 and 5 mb) are shown, as well as a best fit band consistent with the data to one standard deviation.

# Comparing EKS98 and EPS08: $R_{\rm dAu}(y)$

**Stronger shadowing of EPS08 agrees with updated PHENIX d+Au ratio for $y \geq 0$ without absorption but stronger antishadowing disagrees with backward rapidity data**

**For EPS08 to be consistent with data, need a large absorption at backward rapidity with a strong rapidity dependence, inconsistent with most absorption models**

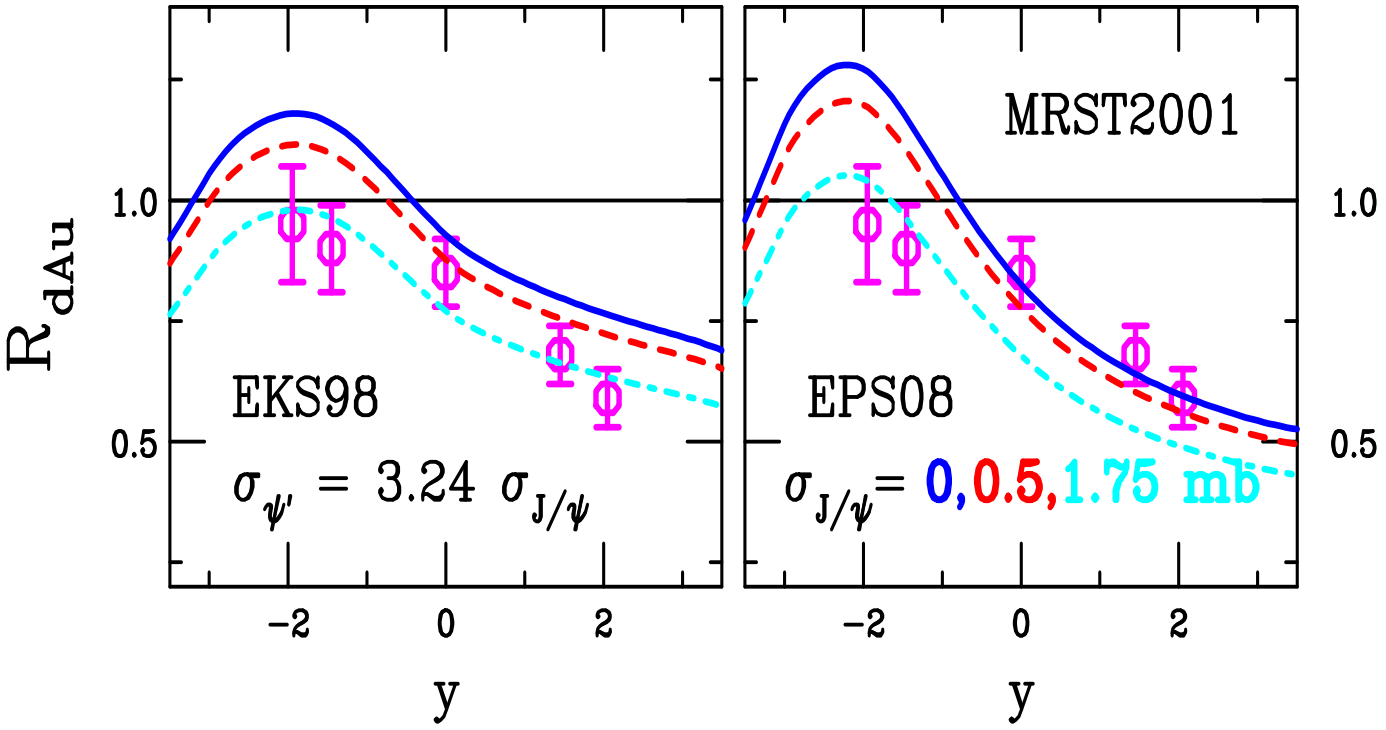


Figure 12: The d+Au/*pp* minimum bias ratio as a function of rapidity for the EKS98 (left) and EPS08 (right) parameterizations.

# Absorption and Shadowing at RHIC: $R_{\rm dAu}(N_{\rm coll})$

**Largest difference between shadowing parameterizations for given $\sigma_{\rm abs}$ is in anti-shadowing region ($y = -1.7$)**

**PHENIX fits using different $\sigma_{\rm breakup}$ in each rapidity interval (the overall best fit cross sections are *not* used)**

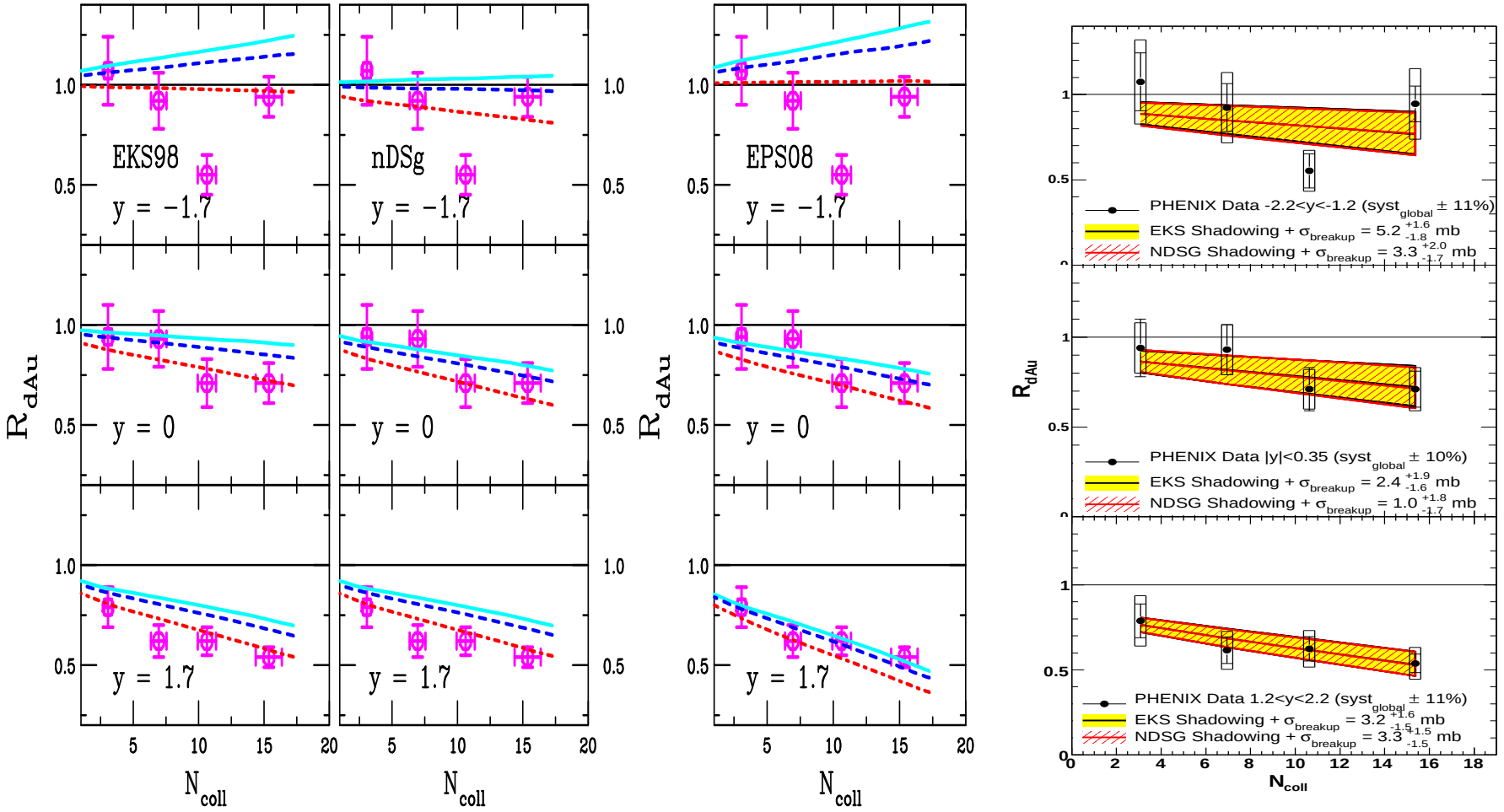


Figure 13: Left: The dAu/$pp$ ratio as a function of the number of collisions calculated with EKS98 (left) and nDSg (right) with the MRST2001 PDFs. The curves are for $\sigma_{\rm abs}^{J/\psi} = 0.5$ (solid blue) and 1.75 mb (dashed red). PHENIX data are shown for d+Au collisions at 200 GeV for $y = -1.7$ (top), 0 (middle) and 1.7 (bottom). Right: PHENIX plot showing the EKS98 and nDSg parameterizations with the breakup cross sections fit in each rapidity interval.

# Absorption and Shadowing at RHIC: $R_{\mathrm{AuAu}}(y)$

**Convolution of shadowing parameterizations give dip at midrapidity**

**Similar effect for nDSg (weaker overall but no antishadowing) and EPS08 (combination of strong shadowing *and* antishadowing)**

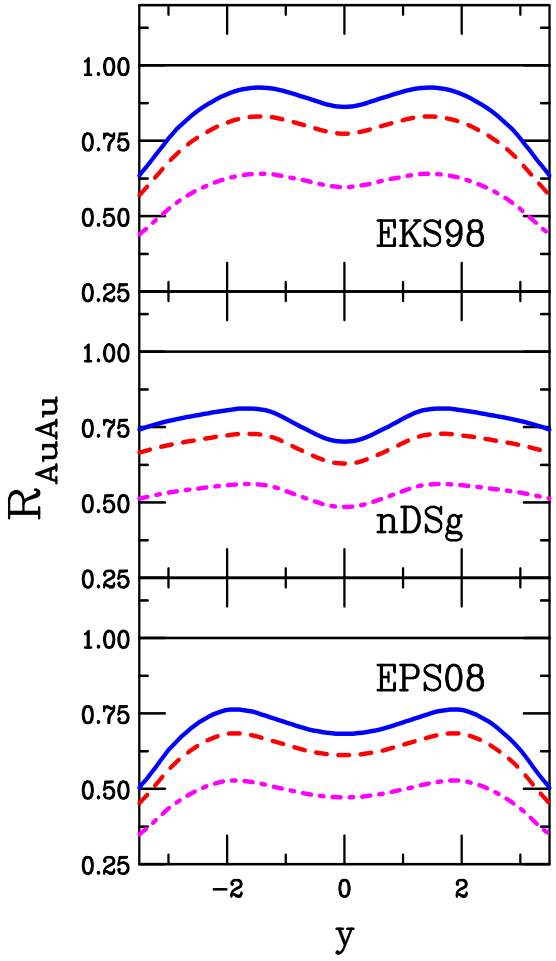


Figure 14: The AuAu/$pp$ minimum bias ratio as a function of rapidity for EKS98 (top), nDSg (middle) and EPS08 (bottom) parameterizations with the MRST2001 PDFs. From top to bottom on each plot, the $J/\psi$ absorption cross section is 0 (solid cyan), 0.5 (dashed blue) and 1.75 (dot-dashed red) mb.

# Why is $R_{\rm AuAu}(y)$ higher at $y = 2$?

**$R_{\rm dAu}$ is lower at $y = 2$ than at $y = 0$ but $R_{\rm AuAu}$ is not**

**Cyan curve is $R_{\rm Aud}$, multiply blue times cyan curves at each $y$ and get magenta curve, including absorption moves all curves down**

**Behavior is a feature of all available shadowing models**

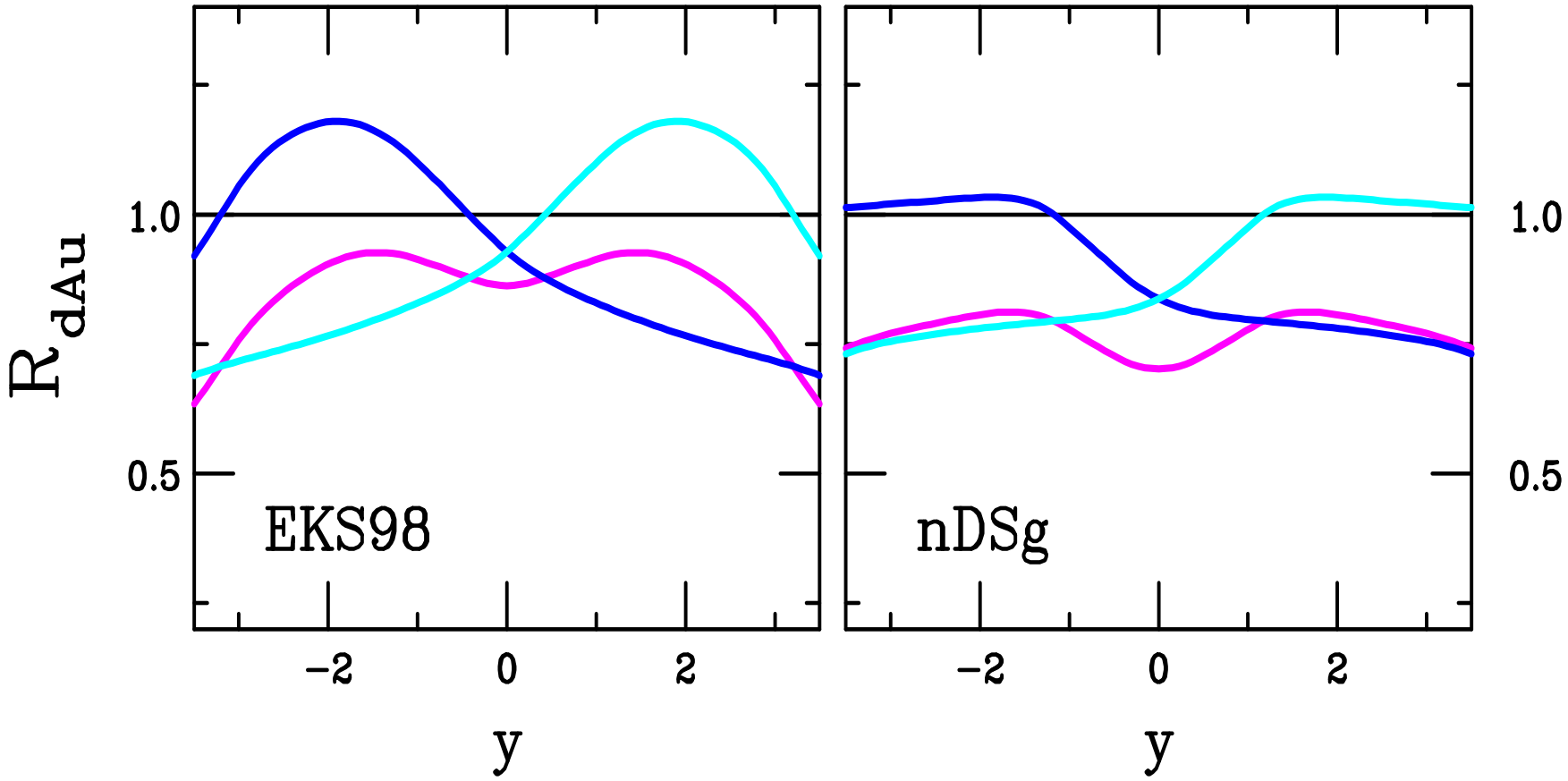


Figure 15: The dAu/*pp* (blue), Aud/*pp* (cyan) and AuAu/*pp* (magenta) ratios as a function of rapidity for EKS98 (left) and nDSg (right) parameterizations with the MRST2001 PDFs.

# Absorption and Shadowing at RHIC: $R_{\rm AuAu}(N_{\rm part})$

**MRST2001 PDFs shown here, GRV98 PDFs take smaller scale and so have stronger shadowing effect, giving stronger $R_{AA}$**

**Much stronger $N_{\rm part}$ dependence at forward rapidity than predicted for cold nuclear matter**

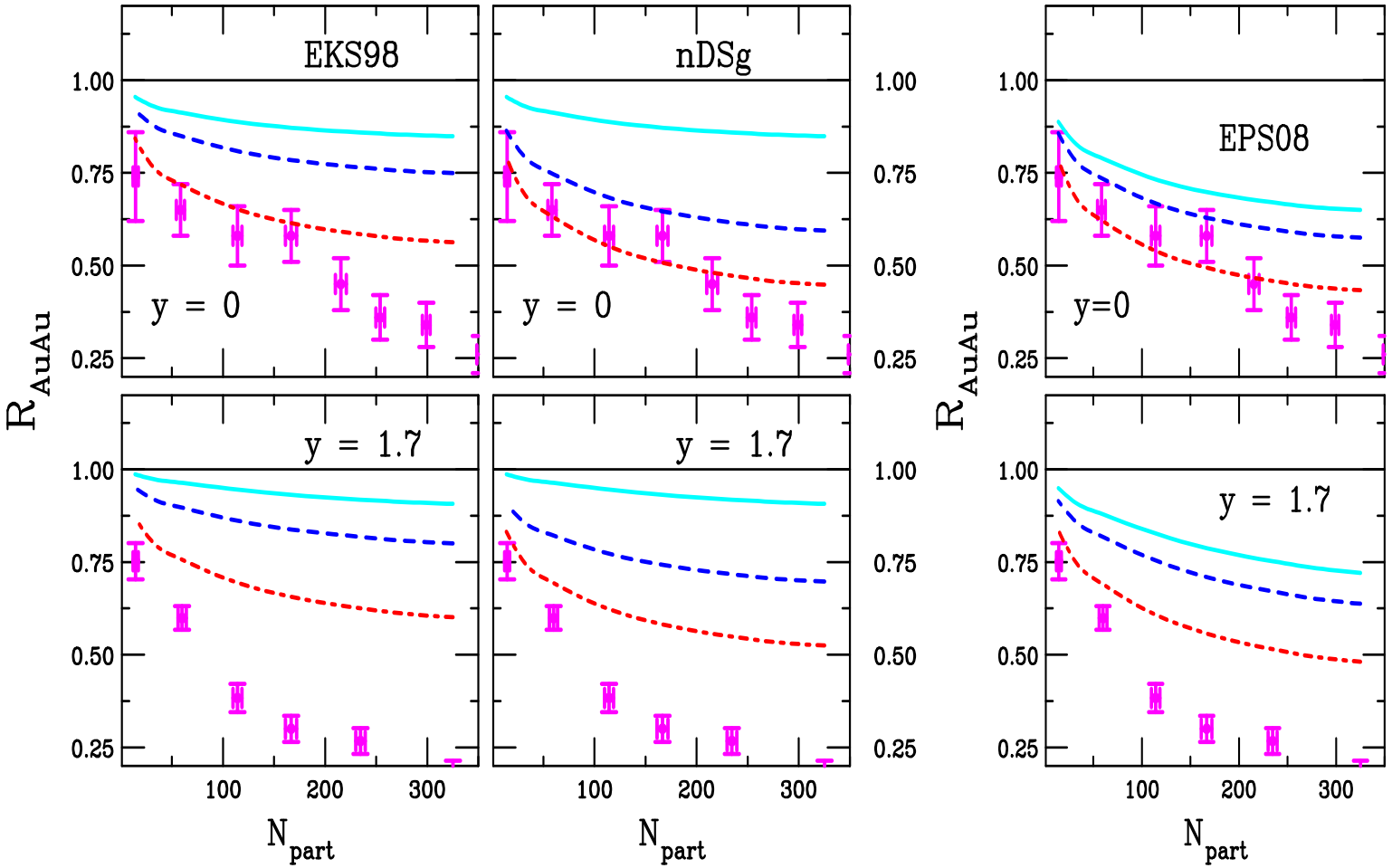


Figure 16: The AuAu/$pp$ ratio as a function of the number of participants calculated with [left-hand side] EKS98 (left) and nDSg (right) and [right-hand side] EPS08, all using the MRST2001 PDFs. From top to bottom on each plot, the $J/\psi$ absorption cross section is 0 (solid cyan), 0.5 (dashed blue) and 1.75 (dot-dashed red) mb. PHENIX data are shown for Au+Au collisions at 200 GeV for $y = 0$ (top), and 1.7 (bottom).

# PHENIX Extrapolation of $\sigma_{\rm breakup}$ to $R_{\rm AuAu}(N_{\rm part})$

**PHENIX d+Au fits to constant "breakup" cross section, $\sigma_{\rm breakup} = 2.8\pm^{1.7}_{1.8}$ mb for EKS98 and $\sigma_{\rm breakup} = 2.2\pm^{1.6}_{1.5}$ mb for nDSg, extrapolated to Au+Au collisions as a function of $N_{\rm part}$**

**Midrapidity data agree fairly well, forward extrapolation does not**

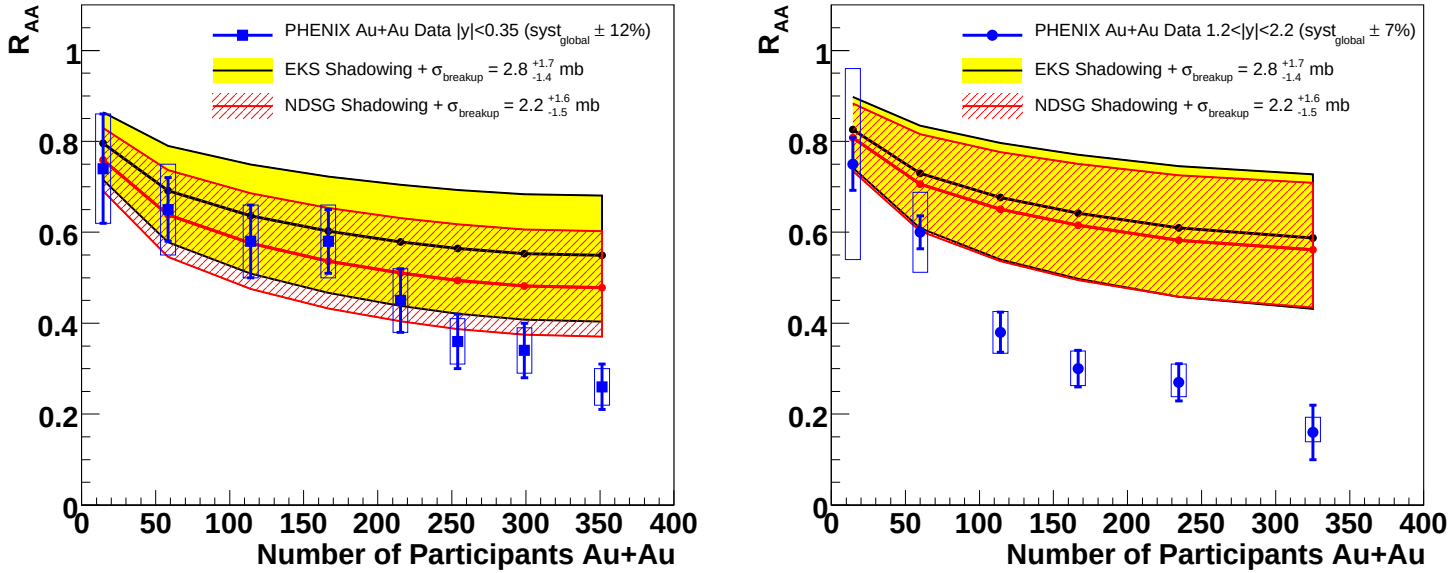


Figure 17: The Au+Au/$pp$ ratio as a function of the number of participants at $y = 0$ (left) and $y = 1.7$ (right). The red and yellow bands show the PHENIX $R_{\rm dAu}$ best fit range extrapolated to Au+Au collisions.

# Absorption and Shadowing at RHIC: Centrality Dependence of $R_{\rm AuAu}(y)$

**Shadowing weaker in peripheral Au+Au collisions but agreement with data for relatively large direct $J/\psi$ absorption cross section, $\sigma_{\rm abs}^{{\rm dir}\, J/\psi} = 1.75$ mb**

**Similar effect for nDSg and EPS08**

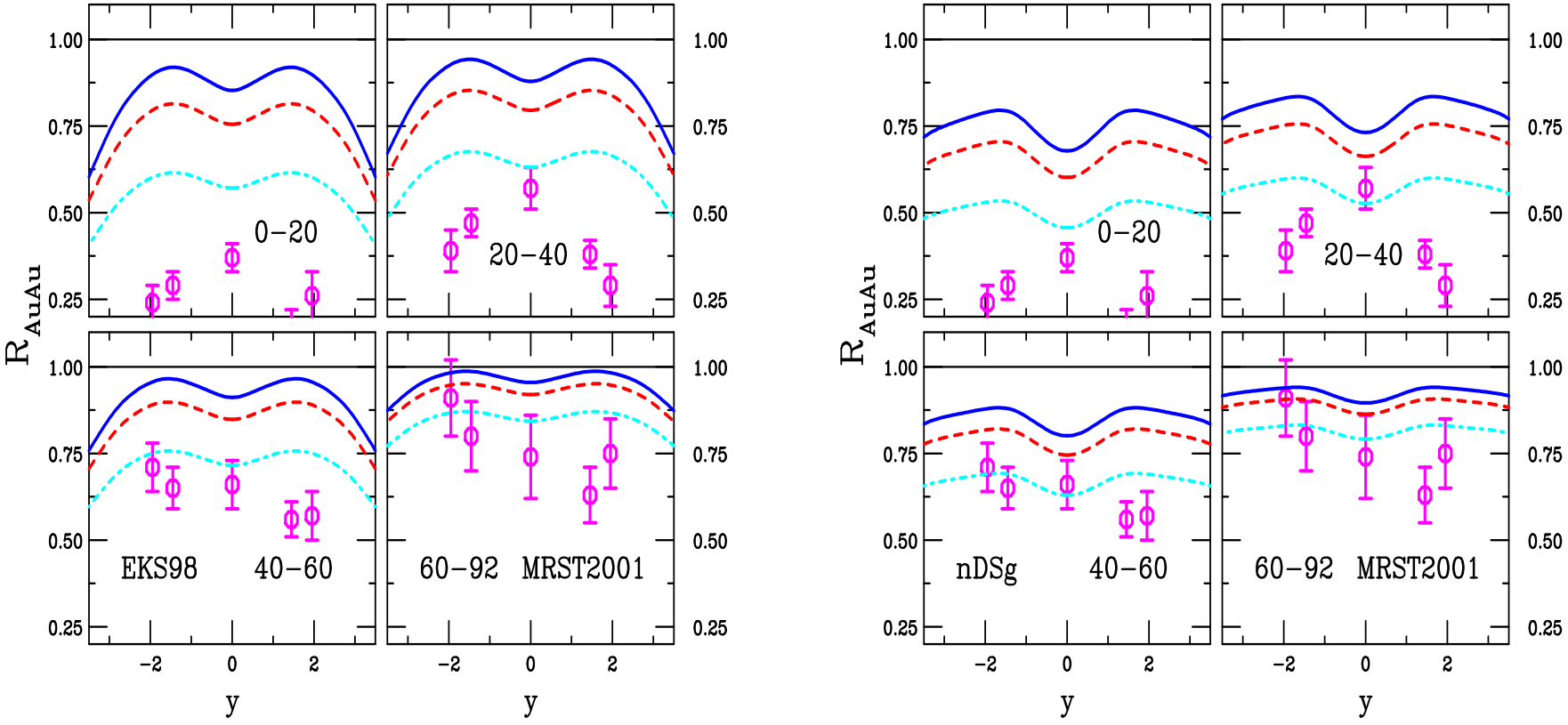


Figure 18: The AuAu/*pp* ratio as a function of $y$ in the four PHENIX centrality bins compared to the data. The calculations with the MRST2001 PDFs are shown with EKS98 (left-hand plot) and nDSg (right-hand plot). The curves are for $\sigma_{\rm abs}^{J/\psi} = 0$ (solid blue), 0.5 mb (dashed red) and 1.75 mb (dot-dashed cyan).

# Absorption and Shadowing at RHIC: $R_{\mathrm{CuCu}}(y)$

**Shadowing effect weaker in Cu+Cu collisions at 200 GeV, all values of $R_{\mathrm{CuCu}}$ are flatter, nDSg considerably weaker for Cu than Au**
**Broad antishadowing peaks for EKS98 and EPS08 at 62 GeV**

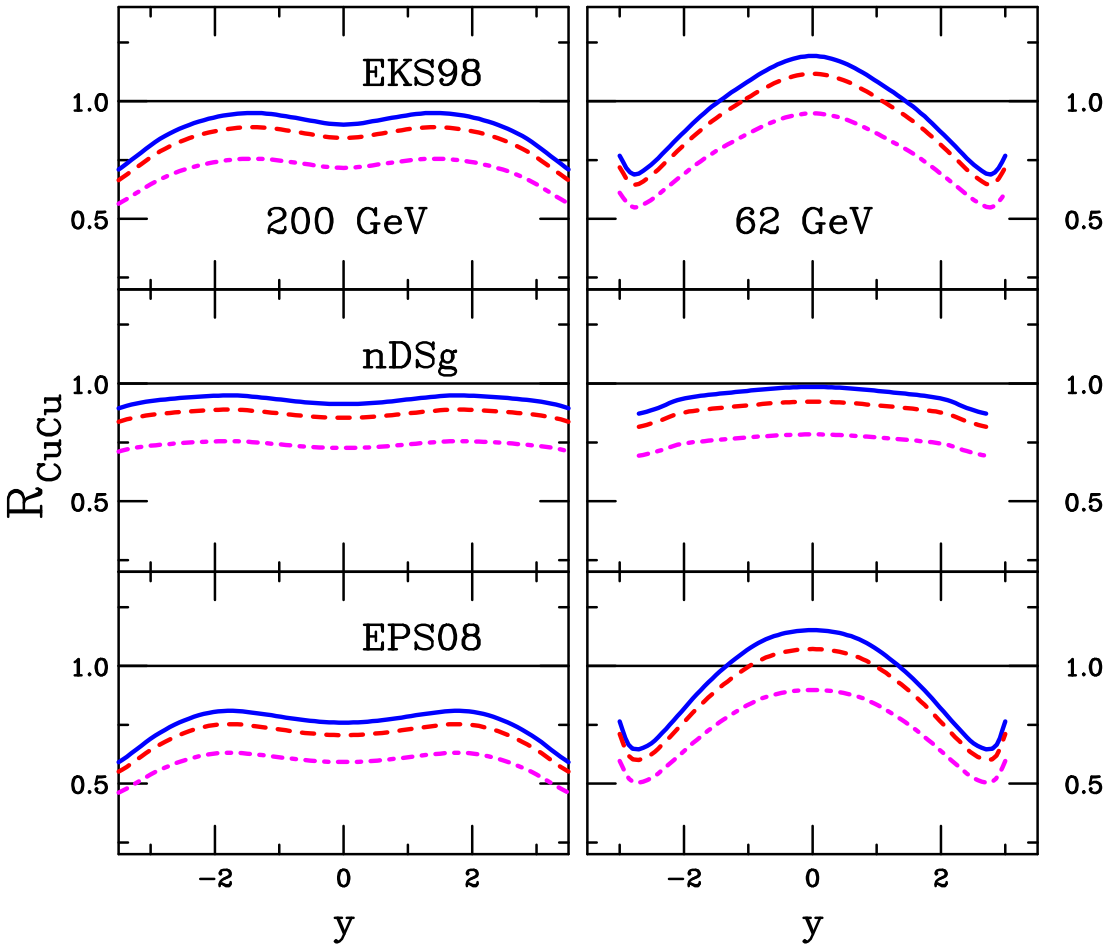


Figure 19: The CuCu/$pp$ ratio as a function of rapidity at 200 GeV [left-hand side] and 62 GeV [right-hand side]. The EKS98 (top), nDSg (middle) and EPS08 (bottom) parameterizations are shown, all calculated with the MRST2001 PDFs. From top to bottom on each plot, the $J/\psi$ absorption cross section is 0 (solid cyan), 0.5 (dashed blue) and 1.75 (dot-dashed red) mb.

# Absorption and Shadowing at RHIC: $R_{\rm CuCu}(N_{\rm part})$

**200 GeV Cu+Cu calculations similar to but weaker than Au+Au**

**At 62 GeV, antishadowing at midrapidity with no absorption, here shadowing stronger at forward rapidity than midrapidity**

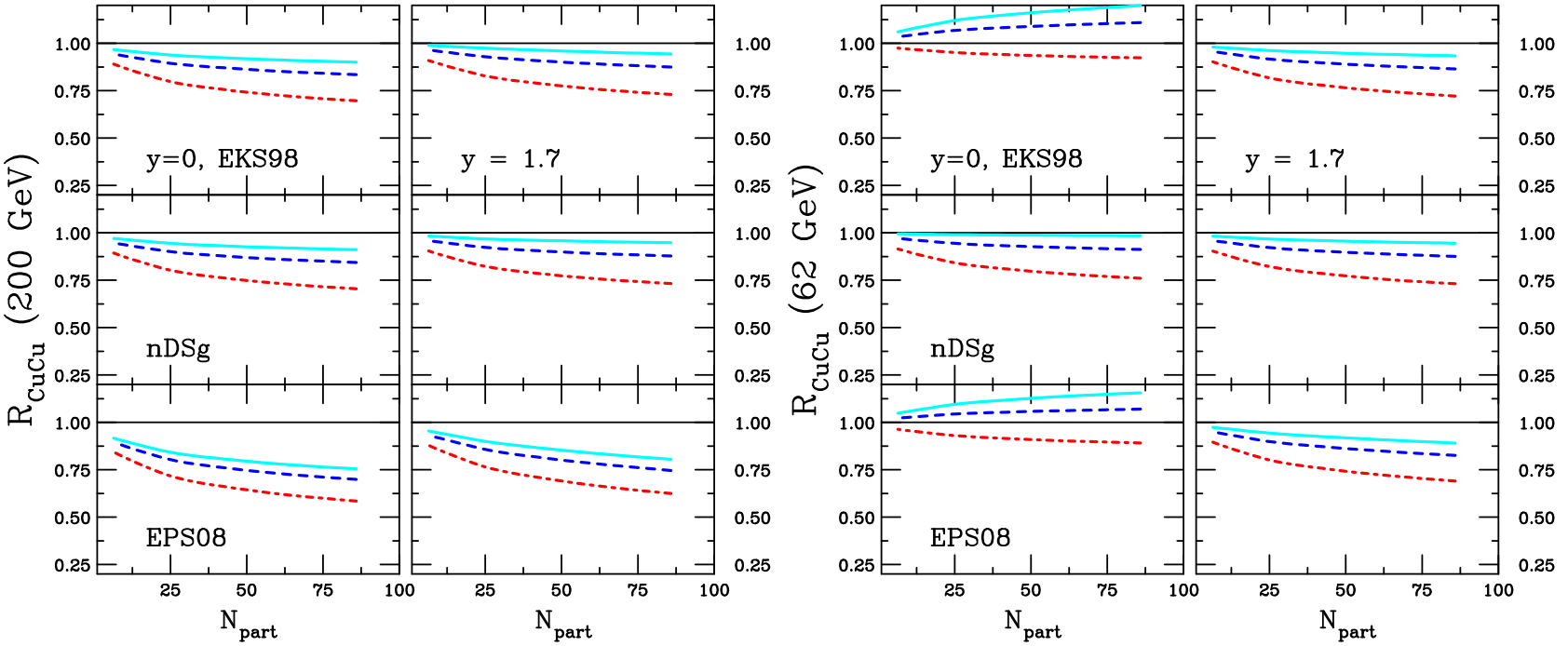


Figure 20: The CuCu/*pp* ratio as a function of the number of participants at 200 GeV [left-hand side] and 62 GeV [right-hand side]. The EKS98 (top), nDSg (middle) and EPS08 (bottom) parameterizations are shown, all calculated with the MRST2001 PDFs. From top to bottom on each plot, the $J/\psi$ absorption cross section is 0 (solid cyan), 0.5 (dashed blue) and 1.75 (dot-dashed red) mb.

# PHENIX Extrapolation of $\sigma_{\rm breakup}$ to $R_{\rm CuCu}(N_{\rm part})$

**PHENIX d+Au fits to constant "breakup" cross section, $\sigma_{\rm breakup} = 2.8\pm^{1.7}_{1.8}$ mb for EKS98 and $\sigma_{\rm breakup} = 2.2\pm^{1.6}_{1.5}$ mb for nDSg, extrapolated to Cu+Cu collisions as a function of $N_{\rm part}$**

**The PHENIX one sigma fit band agrees with data in both rapidity regions**

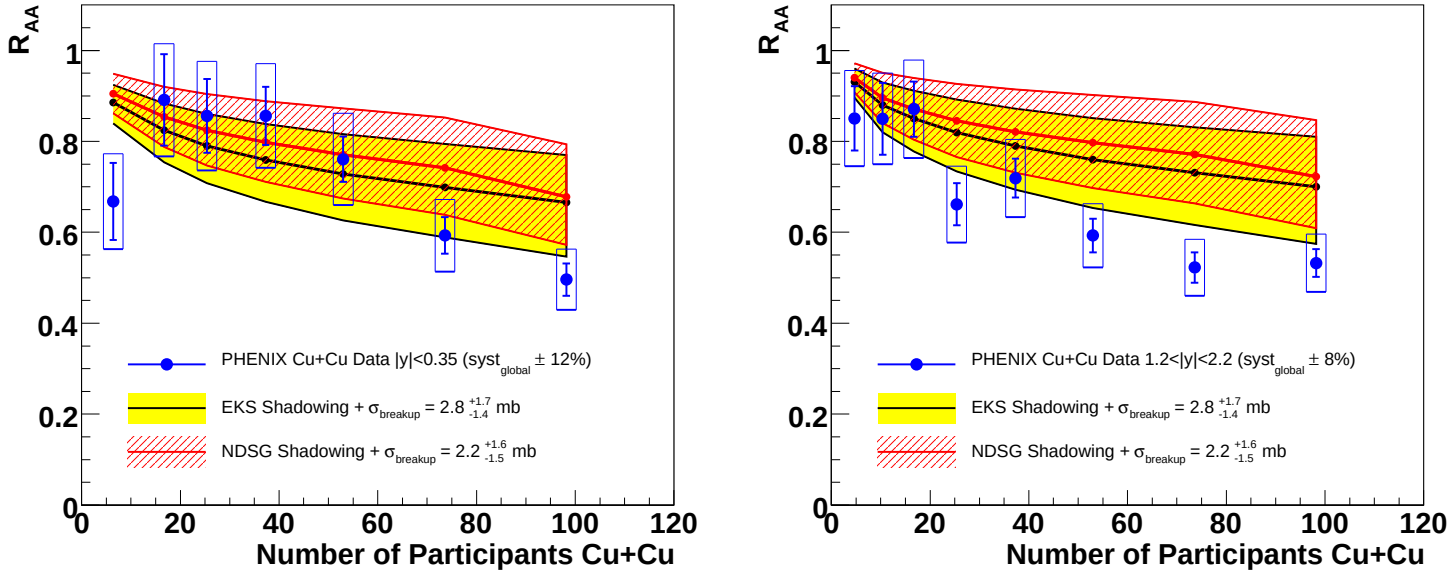


Figure 21: The ratio $R_{\rm CuCu}$ as a function of the number of participants at $y = 0$ (left) and $y = 1.7$ (right). The red and yellow bands show the PHENIX $R_{\rm dAu}$ best fit range extrapolated to Cu+Cu collisions.

# Data Driven Model of $R_{\mathrm{AuAu}}(N_{\mathrm{part}})$

**$R_{\mathrm{dAu}}$ used to constrain modification factor as a function of radial position $r$ in 3 different $x$ ranges, $\mathcal{R}_{\mathrm{low}}(r)$, $\mathcal{R}_{\mathrm{mid}}(r)$ and $\mathcal{R}_{\mathrm{high}}(r)$, corresponding to the forward, midrapidity and backward rapidity ranges of $R_{\mathrm{dAu}}$**

**$\mathcal{R}(r)$ assumed to be linear in $r$ from $r = 0$ to $\mathcal{R}(r \geq 8\,\mathrm{fm}) = 1$**

**$R_{\mathrm{AuAu}}$ is obtained by overlap, $\mathcal{R}_{\mathrm{mid}} \times \mathcal{R}_{\mathrm{mid}}$ at central rapidity and $\mathcal{R}_{\mathrm{low}} \times \mathcal{R}_{\mathrm{high}}$ at $y = 1.7$**

**Data driven model has larger uncertainty but can encompass data in both rapidity regions**

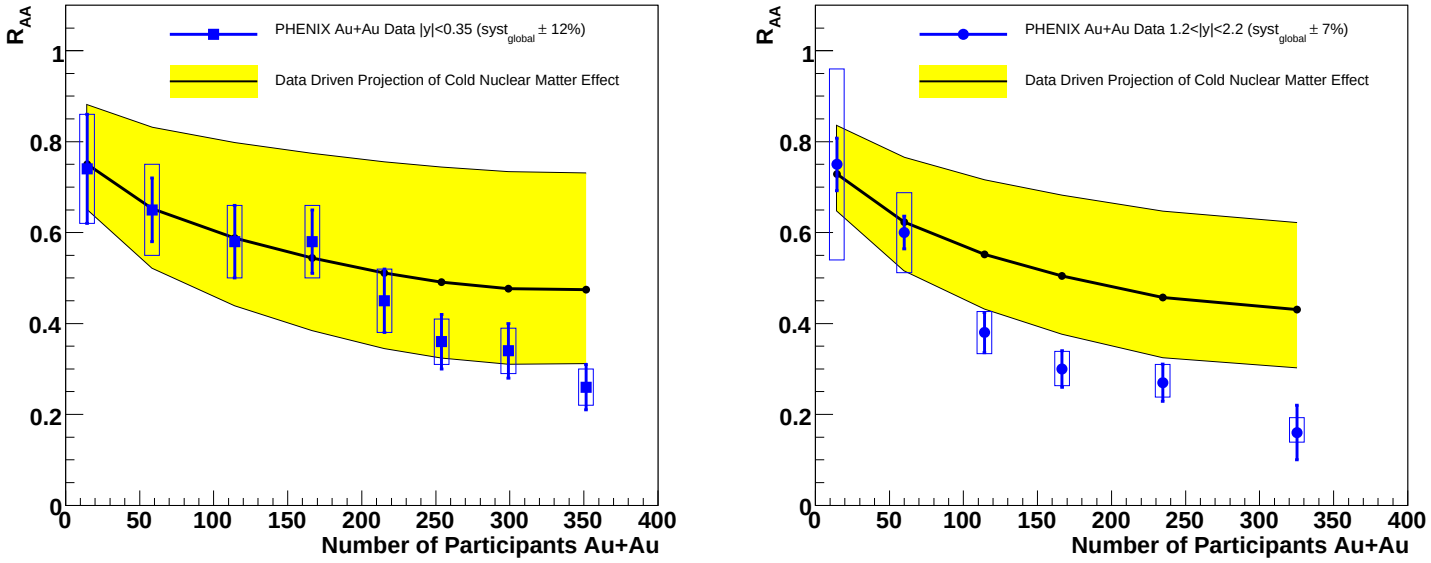


Figure 22: The Au+Au/$pp$ ratio as a function of the number of participants at $y = 0$ (left) and $y = 1.7$ (right) in the data driven model.

# Shadowing Effects on $\Upsilon$ Production: $R_{\mathrm{d}A}(y)$

**Larger $x$ probed for $\Upsilon$ production puts antishadowing peak near midrapidity, narrower $y$ distributions than for $J/\psi$ at same energy due to larger $\Upsilon$ mass**

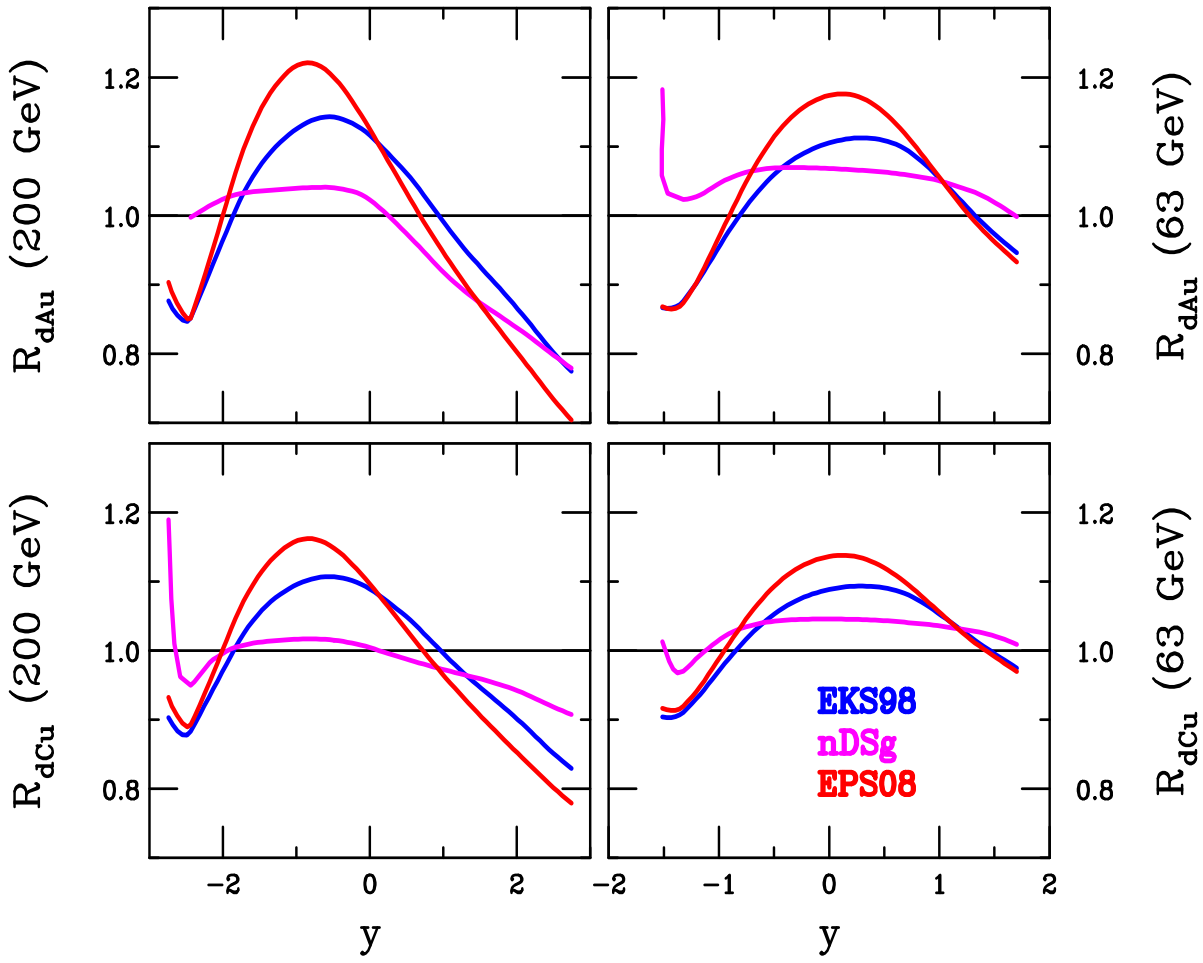


Figure 23: The d+Au/*pp* (upper) and d+Cu/*pp* (lower) minimum bias ratios as a function of rapidity for the EKS98 (blue), nDSg (magenta) and EPS08 (red) parameterizations at 200 (left) and 63 (right) GeV.

# Shadowing Effects on $\Upsilon$ Production: $R_{AA}$

## EKS98 and EPS08 similar for Au+Au and Cu+Cu at 200 GeV, all ratios peak at midrapidity

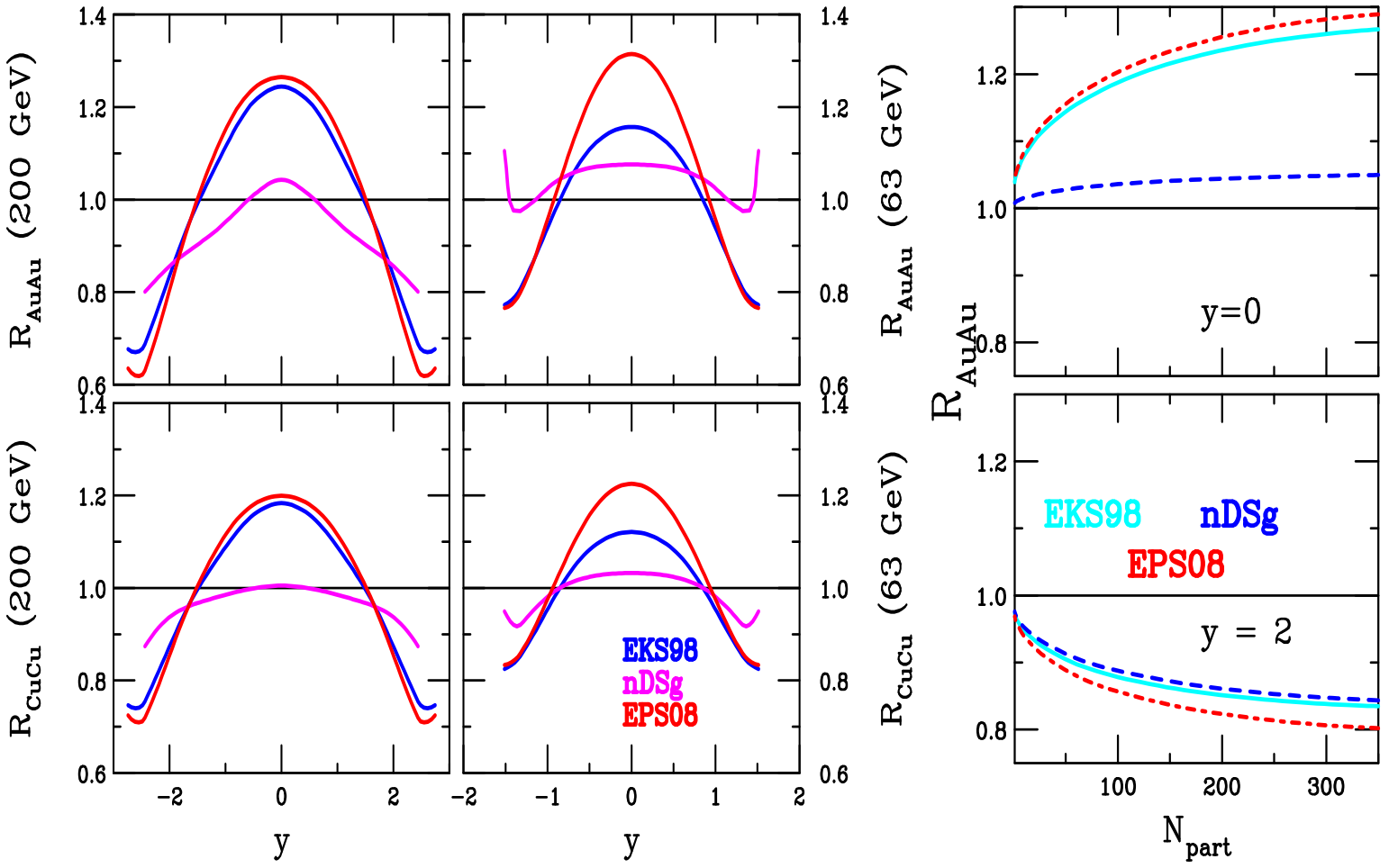


Figure 24: Left: The Au+Au/*pp* (upper) and Cu+Cu/*pp* (lower) minimum bias ratios as a function of rapidity for the EKS98 (blue), nDSg (magenta) and EPS08 (red) parameterizations at 200 (left) and 63 (right) GeV. Right: The $\Upsilon$ $R_{AA}$ for Au+Au collisions at 200 GeV for $y = 0$ (top) and $y = 2$ (bottom).

# Summary

- Data clearly show that $J/\psi$ and $\psi'$ have different $A$ dependence, translates into different effective absorption for $J/\psi$ and $\psi'$
- SPS shadowing and absorption calculations show larger absorption cross sections needed to counter antishadowing effects but $\sigma_{\rm abs}^{J/\psi}$ smaller overall if $\sigma_{\rm abs}^{\psi'} > \sigma_{\rm abs}^{J/\psi}$
- Measurement of $\chi_c$ $A$ dependence would provide additional test of absorption mechanism
- Current d+Au $J/\psi$ data agree well with combination of initial state shadowing and final state absorption
- Data seem to suggest absorption cross section decreases with $\sqrt{s_{NN}}$
- Need better statistics to distinguish between shadowing parameterizations and determine strength of absorption at RHIC – new d+Au data will clearly help
- Cold matter effects need to be accounted for in $AA$ collisions but room for dense matter effects

# Backup

# Predicted $J/\psi$ Rapidity Distributions at RHIC

**Agreement of color evaporation model (CEM) with overall normalization of PHENIX data good**

**Shape has right trend for d+Au with EKS98 shadowing**

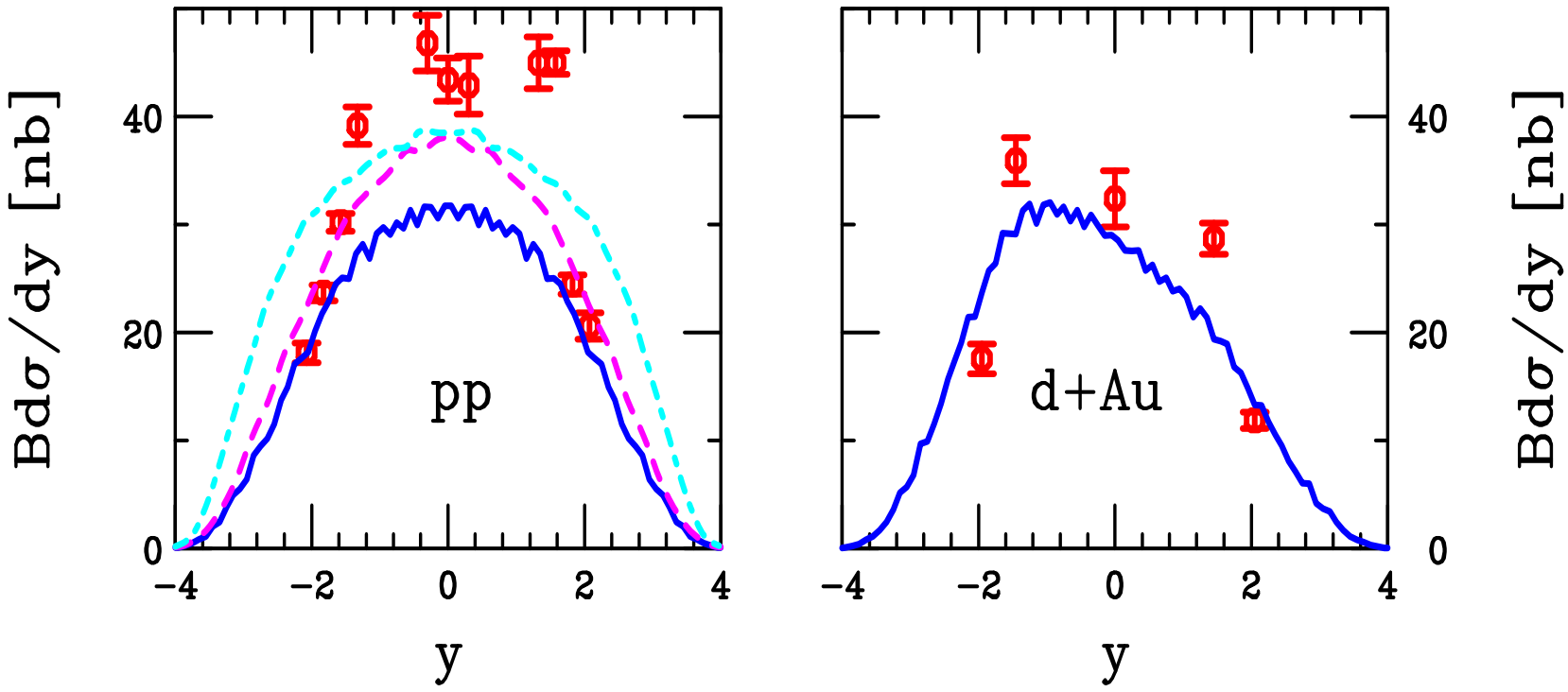


Figure 25: The inclusive $J/\psi$ $y$ distributions in $\sqrt{S} = 200$ GeV $pp$ interactions (left-hand side) calculated with the MRST parton densities in the CEM with $m_c = 1.2$ GeV, $\mu = 2m_T$. The rapidity distribution for d+Au collisions (right-hand side with EKS98) is also shown.

# Including Absorption with Shadowing at RHIC

Effect of changing $\sigma_{\rm abs}$ is shown for the various absorption models

Little difference between constant and growing octet, only at large negative rapidity, singlet absorption only effective for $y < -2$ .

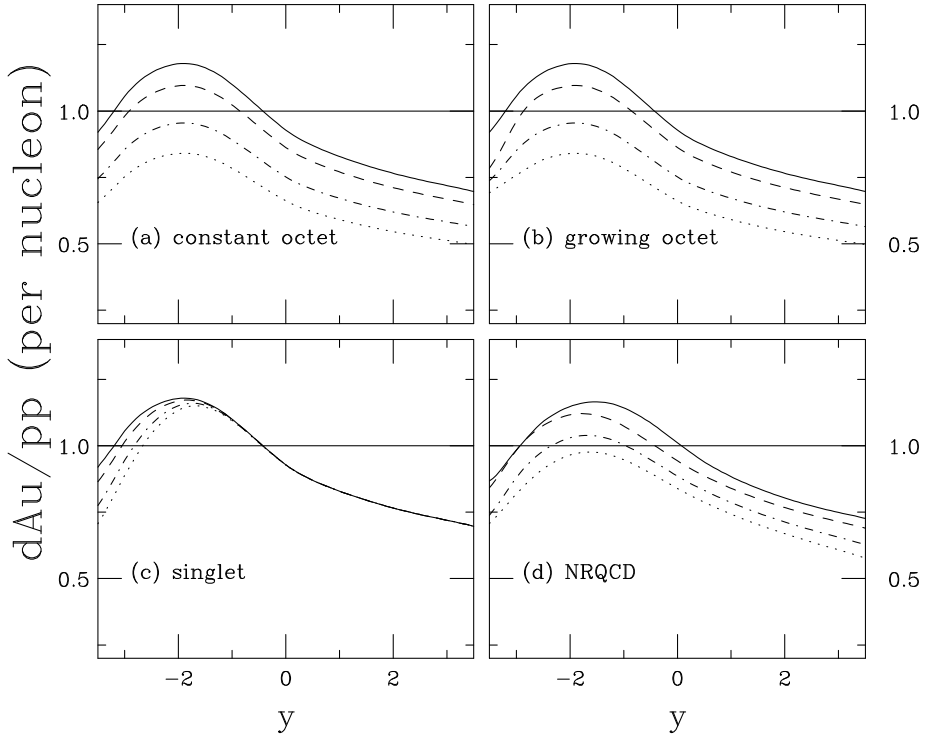


Figure 26: The $J/\psi$ dAu/$pp$ ratio at 200 GeV with EKS98 shadowing as a function of rapidity for (a) constant octet (assuming all states have a constant cross section and do not hadronize in the nucleus), (b) growing octet (states behave as singlets if they materialize in the medium), (c) singlet, all calculated in the CEM and (d) NRQCD with a combination of octet and singlet matrix elements. For (a)-(c), the curves are no absorption (solid), $\sigma_{\rm abs} = 1$ (dashed), 3 (dot-dashed) and 5 mb (dotted). For (d), the results are shown for no absorption (solid, note slight difference relative to the CEM), 1 mb octet/1 mb singlet (dashed), 3 mb octet/3 mb singlet (dot-dashed), and 5 mb octet/3 mb singlet (dotted).

# Obtaining $R_{\mathrm{CuCu}}(y)$ at 200 and 62 GeV

**nDSg parameterization gives less shadowing for Cu than EKS98**

**Lower energy shifts $R_{\mathrm{dCu}}(y)$ toward midrapidity, makes $R_{\mathrm{CuCu}}(y)$ narrower at 62 GeV**

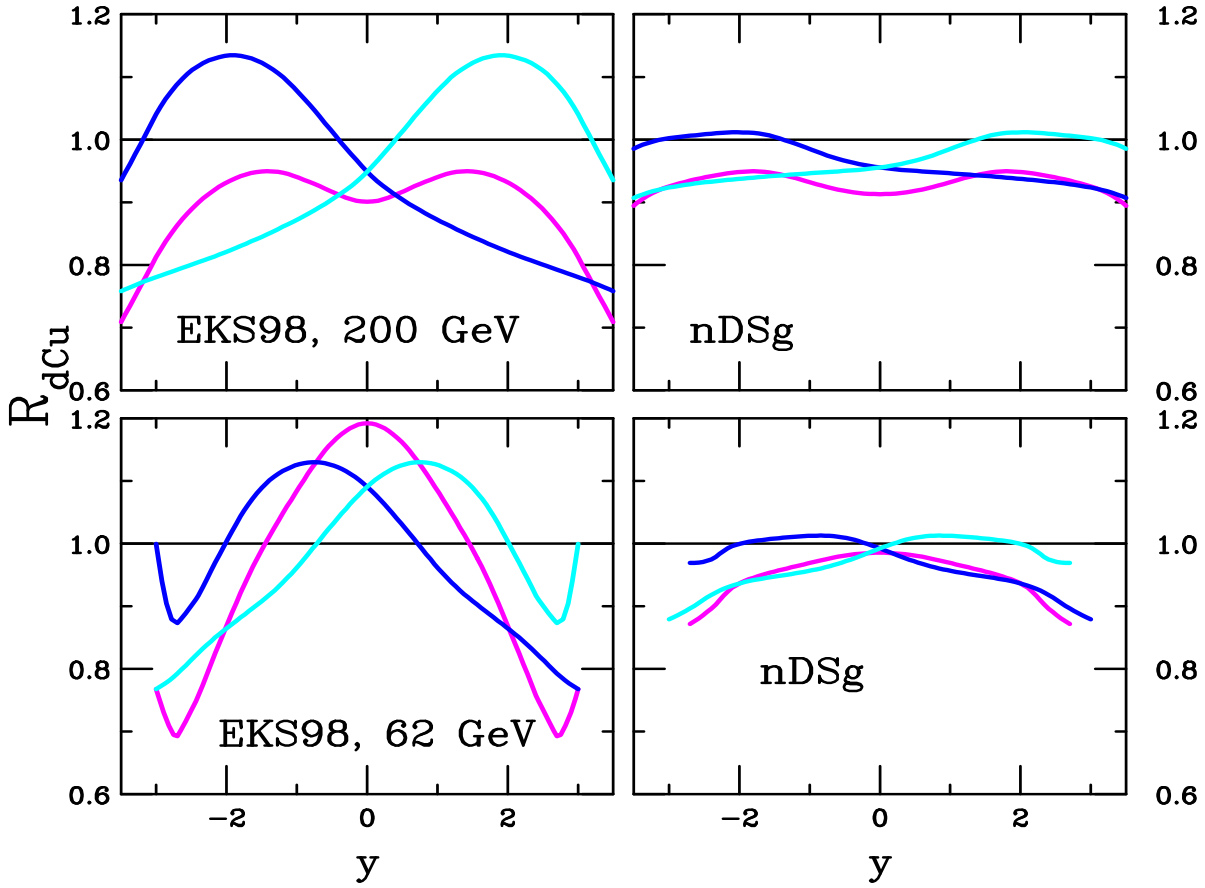


Figure 27: The dCu/*pp* (blue), Cud/*pp* (cyan) and CuCu/*pp* (magenta) ratios at 200 GeV (left-hand plot) and 62 GeV (right-hand plot) as a function of rapidity for EKS98 (left) and nDSg (right) parameterizations with the MRST2001 PDFs. No absorption effects are included.

# How to get $R_{\rm AuAu}(y=2)/R_{\rm AuAu}(y=0) < 1$

**Reduce gluon antishadowing so that $R_{\rm dAu} \approx 1$ at $y = 0$ and shadowing at higher $y$**

**This would also require modifying quark shadowing and satisfying momentum sum rule – no parameterization gives this shape – nDSg comes close but shadowing comes before $y = 0$ and still gives dip at $y = 0$**

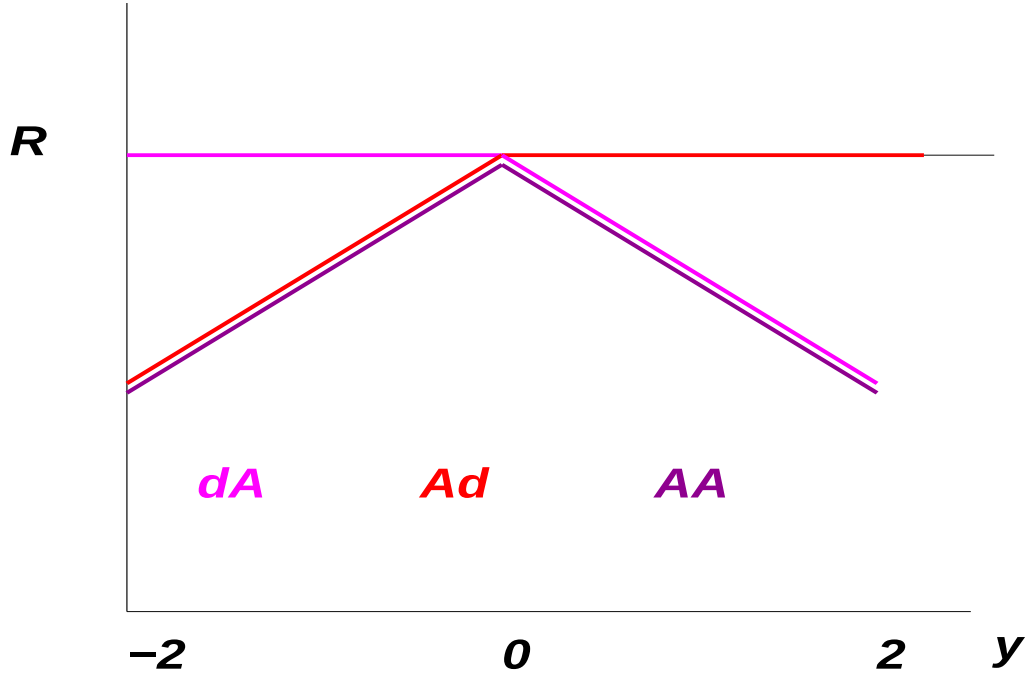


Figure 28: The dAu/$pp$ (magenta), Aud/$pp$ (red) and AuAu/$pp$ (purple) ratios as a function of rapidity to make $R_{AA}(y=2)/R_{AA}(y=0) < 1$